APPLIED SCIENCE DIVISION
Litton Systems, Inc.
2003 East Hennepin Avenue
Minneapolis, Minnesota 55413

INVESTIGATION OF SPUTTERING EFFECTS ON THE MOON'S SURFACE

Eleventh Quarterly Status Report
Contract NASw-751

Covering Period 25 October 1965 to 24 January 1966

Submitted to:

National Aeronautics and Space Administration Headquarters
Office of Lunar and Planetary Programs, Code SL
Washington, D.C. 20546

Submitted by: G. K. Wehner

G. K. Wehner, Director
Surface Physics Laboratory

Prepared by:

G. K. Wehner
D. L. Rosenberg
C. E. KenKnight

Report No. 2957
Date: 8 March 1966
Project: 89308

TABLE OF CONTENTS

INVESTIGATION OF SPUTTERING EFFECTS ON THE MOON'S SURFACE

Eleventh Quarterly Status Report
Contract NASw-751

ABSTRACT

Studies of the Luna 9 photographs imply that the lunar surface is probably cohesive. Using recently published photoelectric data, analysis has been made of the shape of the photometric function of the lunar surface. This analysis indicates the presence of an underdense surface of very small opaque particles. Reconciliation of these indicated properties could be obtained by sintering and cold-welding of the surface material.

The effect of surface roughness on the net ion sputtering rate has been studied again. The decrease in rate with increase in roughness is greater than previously measured. The high sputtering yields of solid graphite when bombarded by hydrogen ions indicate reactive or chemical sputtering is the dominant erosional process and it is unlikely that free carbon will be found on the solar-wind exposed lunar surface.

I. INTRODUCTION AND REMARKS ON THE SOVIET SOFT-LANDING ON THE MOON

A. In This Report

This report includes work from a portion of the twelfth quarter of the present contract in that we wanted to include an analysis of the implications of the Luna 9 soft-landing on the moon and, at the same time, give a complete statement of the implications of the photometric function of the moon. The landing of Luna 9 implies quite a hard surface for the moon in a region that seems in no way unusual. Yet the photometric function of the moon, which is here much more closely defined than ever before with the help of new data and a new method of analysis, sharply demands a tenuous lunar surface. The unification of these demands is treated in the next section.

We have also studied the effect of roughness upon the net erosion rate due to sputtering. The method is a new one and suggests even greater reductions relative to a smooth surface than we have previously measured. On the other hand, we present evidence for greatly accelerated erosion in the case of graphite bombarded by hydrogen ions. Chemical sputtering is implied by these measurements. We describe preparations to study another chemical phenomenon: the formation of H_2O which might result from bombardment of silicates by hydrogen ions.

B. The Lunar 9 Moon Probe and Related Current Literature

The outstanding recent event pertaining to the moon was the soft-landing of the Soviet Luna 9 on 3 February. According to Soviet statements, a 220 lb instrument package of about 2 ft diameter was separated

from the engine section at low altitude so that the rocket exhausts did not influence the area viewed by the camera which was contained in the instrument package. The landing was somewhere in Oceanus Procellarum at a time corresponding to dawn for that region. The cone-shaped instrument package apparently came to rest with its tip pointing toward the rising sun (east in astronautical convention). By deploying four panels making up the tip of the cone, the package nearly righted itself (about 24° off vertical) and, at the same time, exposed a short periscope turret on the instrument axis. A panorama of pictures were taken from this turret and were subsequently relayed to earth. The four panels were not deployed symmetrically with respect to the instrument axis, because the tip of a panel appears only in one view, the one looking scuth. The view to the west was not released as it did not view any of the surface of the moon. The view to the east is the most interesting, of course, as it gives a close-up view of the surface.

No details have yet been released on the angles subtended in the Soviet photographs. But the angles in the photographs can nevertheless be estimated as follows. From the shadow patterns in the published photographs, the general direction of the view can be ascertained. There are 6 full frames that apparently complete a panorama of 270° from northwest to southwest with negligible overlap or gaps. Then the frames are 45° in width. If so, the frames are 30° in height. The central axis tilt of 24° follows from the tilt of the horizons in the southerly and northerly directions. Internal consistency of these estimates is assured by measuring the apparent change in the elevation of the horizon when viewed

in adjacent frames. For a change in azimuth by 45° with the instrument tilted by 24° from the vertical, the horizon should shift by about 20° in the elevation direction on the frames. From the south and southwest frames, the measured shift is 22°, while for the north and northwest frames, it is 19°.

The linear scale in the photographs follows if the height of the turret can be estimated. One estimate is afforded by the Soviet statement that the pictures show a horizon at a radius of about 1 mile. This was surely the result of a calculation in which the moon was approximated by a perfect sphere. Using this approximation, an object 70 cm above the surface of a sphere of 1740 km radius "sees" its horizon at 1.55 km or 0.96 mile. If one adopts a turret height of 70 cm, then, for example, the view to the east at 9° to 39° below the horizontal permits the identification of 4 to 1 cm in detail, respectively (10^{-2} radians). A turret height of 70 cm requires that the 2 ft diameter sphere is hardly buried. Reduction of the turret height proportionally reduces the linear scale of the surface detail.

A significant result of the Soviet picture-taking mission is that the turret is obviously well above the surface, namely, that the surface of the moon is sufficiently firm so that a sphere weighing about 37 lb in the lunar gravity was hardly buried. Of course, the impact force was at least an order of magnitude larger than the 37 lb weight. The residual velocity was "a few meters per second" according to the news release. Deceleration in 0.3 m from 5 m/sec, for example, requires an acceleration of the order of 40 m/sec^2. A speed of 5 m/sec would result from a fall of

only 7.5 m in the lunar gravity. In English units, the package developed some 10^3 lb of force over about 2 ft^2. The "bearing strength" (thus loosely defined) is of the order of 500 lb/ft^2 or 4 psi in that locale (1 lb/ft^2 = 478.8 $dyne/cm^2$).

On the other hand, the close-up view of the surface in that locale reveals a spongy surface on a centimeter scale. With very few exceptions, the shadows in the surface are of length comparable to width despite the low angle of the sun. This means that the surface is full of voids. Only a few objects projecting from the surface can be identified by their long shadows. This virtual absence of positive relief features is in agreement with the Ranger series of photographs so that the locale of Luna 9 cannot be considered to be unusual in any obvious way. That it is spongy is surely no surprise.

Later in this report we emphasize that the photometric function of the moon very certainly requires that virtually all of the surface is an underdense powder. In fact, the powder has to be underdense in the sense that the individual powder grains cannot be packed down in the manner that a gravel-pile packs itself. This means that the open surface structure on a centimeter scale that was revealed by Luna 9 is itself made up of an open microstructure on a 0.1 mm scale or smaller. Hapke and Van Horn[1] estimated that 60 μ particles were the largest that would not suffer gravel-pile packing in the lunar gravity field.

Other evidences for a tenuous surface layer could be cited. In a recent review Ruskol[2] cites, for example, the time constant for temperature changes (both infrared and radio frequencies), the limb darkening in

thermal emissions from the moon, and the reflectivity in radar measurements. Several of these effects require a fairly tenuous layer to a depth of several tens of meters. It could be mentioned that Jaffe[3,4] has supported the suggestion by several of the members of the Ranger experimental team that the nearly unanimously rounded appearance of the lunar craters having about 100 m diameter implies the presence of an overlay of 5 to 10 m of granular material. In studies of model craters, Jaffe is able to closely match the profiles of model craters to those of Mare Cognitum by sifting a layer of sand over the model craters.

A new evidence for a tenuous surface layer has been given by radar specialists of MIT's Lincoln Laboratory. From data at 23 cm wavelength, Hagfors et al.[5] conclude that most of the moon has an upper layer of low density and having a thickness at least in excess of their radar wavelength. The effect they study is, in fact, closely related to the limb darkening in thermal emission from the moon. At oblique incidence, the absorption in a tenuous upper layer is expected to be different for waves linearly polarized in, and perpendicular to, the local plane of incidence of the wave. The underlying layer is expected to backscatter the two polarizations equally. They find a systematic difference in the two polarizations for most of the moon but not, for example, for the ray crater Tycho. The data imply a dielectric constant ϵ = 1.7-1.8 for most of the moon. This value is in very good agreement with the dielectric constant inferred from limb darkening of the thermal emission at similar wavelength. Tycho is also anomalous thermally, and must have, at most, a thin upper layer.

The lunar dielectric constant inferred from the radar reflectivity in a one-layer model is significantly higher than that given by the radar method at oblique incidence. But the two radar results can be reconciled if the underlying layer in a two-layer model is solid rock. The depth to the solid rock would be 5 to 10 m if the increase in radar reflectivity at 10 to 20 m wavelengths found by Davis and Rohlfs[6] were considered to be real. Unfortunately, the uncertainties in the lunar reflectivity are so large that little confidence can be assigned to differences between the measured reflectivities.

Davis and Rohlfs and earlier workers unequivocally established that there exists a wavelength dependence of the reflected power at various delays (angles of incidence) relative to the initially returned power. As suggested by Evans,[7] the moon displays a central bright spot that contracts and brightens with increasing wavelength of the radar. This result has traditionally been interpreted as evidence for a sandy, desert-like surface of fairly gentle undulations with a few rocks strewn over it to act as discrete scatterers at oblique incidence. It should be clear that this wavelength dependence of the reflected power at varying angle of incidence also gives some information on the make-up of what lies within the overlying tenuous layer. At decameter wavelengths the overlying layer looks quite smooth to the radar, while at shorter wavelengths it is relatively rough. This suggests that the tenuous layer is relatively "grainy" at centimeter wavelengths but increasingly homogeneous at meter and decameter wavelengths. This suggestion is supported by the virtual absence of any visible objects of 10 cm dimension or larger in the Luna 9

photographs. Obviously a large body of data predicted a spongy surface in those photographs.

The density of the overlying tenuous layer that is required by its thermal inertia, radar backscatter, and optical backscatter is in the neighborhood of 0.5-1.2 gm/cm^3. Can a low density substance have such "bearing strength" as the 2-3 x 10^5 $dyne/cm^2$ estimated above? For comparison, we analogously analyzed the "bearing strength" of poured, self-compacting powders into which we dropped glass spheres. Burial of nearly half the sphere implied an estimated "bearing strength" of the order of 10^5 $dyne/cm^2$. Sifted, non-compacting powders (that give better agreement with the moon photometrically) would have lower "bearing strength" by an order of magnitude. The discrepancy in bearing strength between these cohesionless powders and the moon's surface is not large but may be real. On the other hand, the impact of Luna 9 at a few meters per second in a cohesionless powder would cause a considerable splash of displaced material to several package diameters. But scrutiny of its photos reveals no apparent change in the surface appearance between 1 and 5 m from the craft. In fact, it would be difficult to believe that a cohesionless powder could come to rest with the open structure seen in the 1-5 m radial zone around Luna 9.

The material into which Luna 9 impacted is probably, therefore, cohesive. If it is powdery as required by the argument for a tenuous surface, the powder could become cohesive by being sintered or welded at the interparticle contact points. A paper on sintering of lunar dust was just published by Smoluchowski.[8] He emphasizes that two factors

at the moon's surface should contribute to sintering of dust. There must be a means of making crystal lattice defects available (vacancies or interstitials, particularly). Once the defects are available, there must be adequate thermal agitation to move them to the crystal surface. He makes the point that surface temperatures are adequate for motion of interstitials, at least. Motion of vacancies in insulating crystals is less certain. As to a source of lattice defects, he tends to favor solar particles of MeV energies and higher. He felt that cohesion arising from solar-wind ions through cold-welding due to sputtering or through sintering due to crystal damage was apt to require doses corresponding to about 10^5 yr of unperturbed exposure. We feel that such time periods of unperturbed exposure may indeed be possible on the basis of our studies[9] of the darkening rate of powders subjected to a simulated solar wind. In the equivalent of 10^4 yr of exposure to the solar wind, we invariably find a detectable increase in cohesion of the surface particles. In the same time period our sample albedos are decreased to lunar albedos for many rock materials. In times equivalent to 10^5 yr, a number of materials become decidedly darker than any known lunar albedo. Whether our increase in interparticle cohesion is adequate for very underdense powders to agree with the lunar "bearing strength" will be the subject of future research.

II. SPUTTERING YIELD REDUCTION DUE TO SURFACE ROUGHNESS

A knowledge of ion bombardment sputtering rates for likely lunar surface materials is important with respect to estimates of the amount of material moved and possibly removed from the lunar surface by action of the solar wind. Most published sputtering yield data were obtained for smooth surfaces,[10] but it is known that surface roughness can result in a greatly reduced yield. Last quarter, in connection with our argon bombardment of porous nickel disks, it was noted that the sputtering yield for the porous nickel under 400 eV argon ion bombardment was 0.6 atom/ion, about one-half that expected for a smooth solid Ni surface. Several years ago, in bombardment studies with threaded nickel cylinders, we found that yields were reduced up to more than 50% due to re-attachment of sputtered atoms, especially at the lower ion energies. In an effort to carry surface roughness to an extreme, we have determined the sputtering yield of a surface composed of the points of common sewing needles for 500 eV mercury ion bombardment.

The needles in our sample are 0.76 mm in diameter and made of a nickel-plated steel. Several hundred of them are tightly held in a glass cylinder, with only the ends being exposed to the plasma. Figure 1 is a picture of the target configuration after a considerable amount of material was sputtered away. The needle ends became blunt and at the sample edge, under more oblique ion bombardment, wedge shaped. The target was bombarded for 24 hr by 500 eV mercury ions with a 3.2 mA/cm^2 ion current density. The average weight loss was 5.5 mg/hr. The same target was subsequently bombarded for an additional 24 hr with an average weight

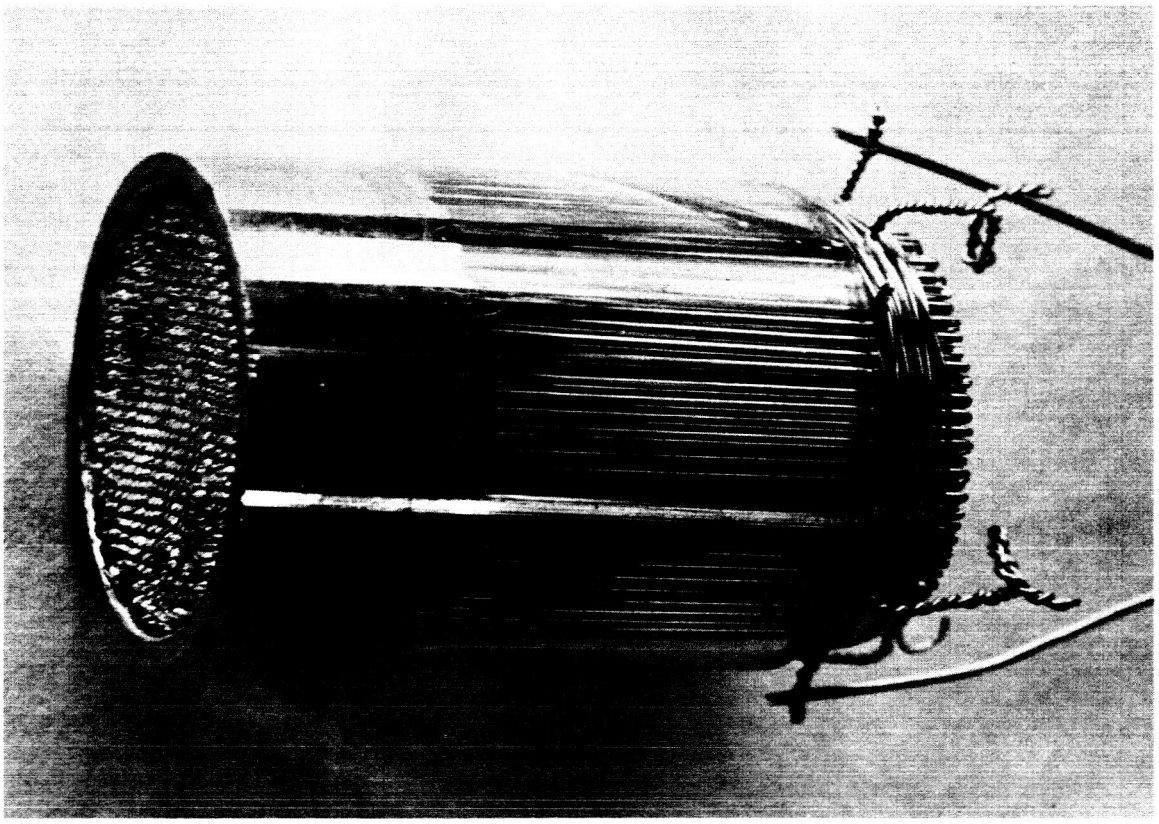

Fig. 1 Sewing needle target configuration after ~48 hr Hg sputtering.

loss of 6.9 mg/hr. For comparison purposes, a No. 1020 cold-rolled steel slug was mounted in the same size glass shield and subjected to bombardment conditions identical to those of the needles. The resultant average weight loss was 16.6 mg/hr. These yields indicate that the needle surface configuration has a sputtering yield of approximately 1/3 that of a smooth solid surface. The increasing erosion rate as the needle points became blunted indicates that roughness might have initially reduced the net sputtering yield to less than 1/3 of that for a smooth surface.

Judging from the threaded nickel cylinder studies, bombardment at ion energies lower than 500 eV would result in still smaller ratios of rough to smooth surface yields. This dependence of the effect of roughness on ion energy is related to the changing angular distribution of sputtered atoms. For ion energies below a few hundred electron volts, sputtered atoms are relatively less numerous perpendicular to the surface than for higher ion energies.[11] But above about 500 eV, the angular distribution is nearly $\cos\epsilon$, just as it has been found to be for H^+ ions of solar-wind energies impacting on Ag.[12] We therefore believe these findings for 500 eV Hg ions are directly comparable to roughness effects experienced in solar-wind sputtering.

These findings, applied to the very rough and porous layer surface, indicate that solar-wind sputtering yield estimates probably should be revised downward. In our published estimate[13] an allowance of 1/2 was made for the effect of roughness.

III. CHEMICAL SPUTTERING OF GRAPHITE

In 1926 Guentherschulze[14] observed that hydrogen ion bombardment may, with certain materials, give rise to chemical or reactive sputtering with larger yields than in physical sputtering. In order to more quantitatively determine the extent of this chemical sputtering effect, solid graphite was bombarded by hydrogen ions from an rf supported hydrogen plasma. A slug was formed from a spectrographic grade graphite electrode and dc bombarded by hydrogen ions with energies of 200, 400, and 600 eV and current densities of from 2 to 4 mA/cm^2. The graph of yield vs ion energy in Fig. 2 shows that the resultant hydrogen sputtering yields are at least one order of magnitude higher than would be expected for physical sputtering. Yield curves are also given for helium and argon bombardment for comparison purposes. The slope as well as the magnitude of the yield curve for hydrogen indicates chemical sputtering effects. Possibly some of the increase in yield with ion energy can be attributed to target temperature and chemical reaction rate increase with increasing ion energy. Interestingly, the yield approaches unity. This means that each hydrogen ion causes the removal of one carbon atom. The relative contribution of H^+, H_2^+, and H_3^+ are not known, however. The high carbon sputtering rates under solar-wind bombardment make it unlikely that one will find free carbon on the solar-wind exposed lunar surface.

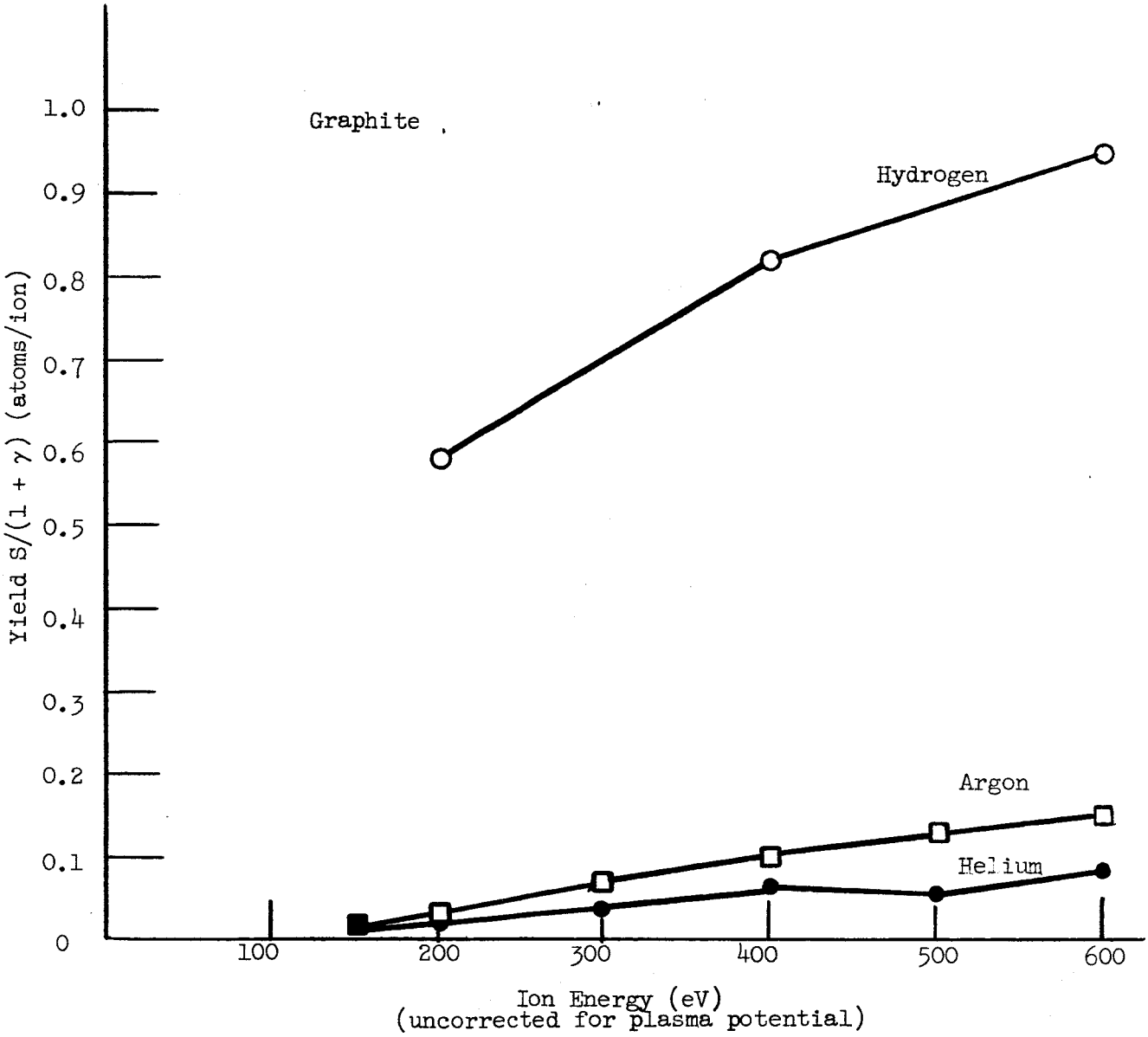

Fig. 2 Sputtering yield vs ion energy for solid graphite.

IV. WATER FORMATION BY SOLAR-WIND BOMBARDMENT

We are just beginning experiments to ascertain to what extent the solar wind might have contributed to the formation of water molecules.

A liquid nitrogen cooled cold finger and a Consolidated Electrodynamics Corporation Type 21-611 Residual Gas Analyzer are presently being installed in our hydrogen plasma ion bombardment vacuum system. By comparing water evolved from the cold surface after equal periods with and without sample bombardment, we hope to be able to detect the presence and extent of any water molecule formation due to the hydrogen bombardment of a powder sample. The recent work by Blauth and Meyer[15] on the formation of water molecules due to the attack of glass by atomic hydrogen is of much interest in this connection. Such H_2O formation should saturate after removal of a fraction of a monolayer of oxygen. Clearly such H_2O formation is of little consequence for the moon because a monolayer of oxygen removed from all the surface of all the close-packed 50μ spheres in a 1 cm^2 column 1 m high would yield only about 2 mg of water. Since the mass of released water depends on only the first power of the assumed particle diameter, the estimate is not very sensitive to choosing 50μ spheres.

However, in the presence of sputtering, new surfaces are being continually exposed. Therefore as much as a few percent of the oxygen contained in a 10 ▪ thick layer on the moon might have been converted to H_2O. Barring unforeseen difficulties, we hope to report the results of this experiment in the next quarterly report.

V. THE PHOTOMETRIC FUNCTION OF THE MOON

A. Introduction

A large number of lunar photometric data in tabular form were recently published by Gehrels, Coffeen, and Owings[16] (GCO). These data, obtained photoelectrically, offer an unprecedented opportunity to closely define the function governing the intensity of light scattered from 11 selected regions of the moon.

Some analysis of the photometric data was made in GCO in terms of the theory proposed by Hapke.[17] Unfortunately, the photometric function of Hapke is invalid because of a mathematical error and at least two mathematical procedures that are not physically tenable, as will be discussed below.

We have completely re-analyzed the photometric data of GCO. In addition, these data on individual features have been compared to the brightness of the whole moon as measured by Rougier[18] after putting the two sets of data on the same basis. The excellent agreement of the whole moon data with that of most of the 11 lunar features confirms the validity of our procedure.

The thus closely defined photometric function of the moon will be compared with that of powder samples darkened by a simulated solar wind. A qualitative theory of the lunar photometric function will be offered. It will be shown that the numerous previous suggestions that the surface of the moon has a tenuous surface of small particles is given emphatic support by these new photometric data and this new analysis procedure.

B. Analysis of Photoelectric Photometry of the Moon

1. Procedure

The suggestion was made by Hapke[17] that it is valid to factor the lunar photometric function $I(i,\epsilon,\alpha)$ into a function $L(i,\epsilon)$ of angles of incidence i and of emergence ϵ and a second function $F(\alpha)$ that depends on phase angle α only. He separated the second function into another product $F(\alpha) = S(\alpha)B(\alpha)$, where $S(\alpha)$ describes how an average particle scatters light and $B(\alpha)$ results from shadowing within a tenuous surface of small, opaque particles. However, no experimental separation of $F(\alpha)$ into two functions can be accomplished for lunar data, so our attention shall be confined to $F(\alpha)$.

The function of incidence and emergence $L(i,\epsilon)$ that was suggested by Hapke is the Lommel-Seeliger function

$$L(i,\epsilon) = (1 + \cos\epsilon \sec i)^{-1}$$
$$= \cos i/(\cos i + \cos\epsilon) . \qquad (1)$$

There has been no previous test whether the proposed factoring of $I(i,\epsilon,\alpha)$ is valid. The observational data on individual features correspond to values of $I(i,\epsilon,\alpha)$. A test of the factoring of $I(i,\epsilon,\alpha)$ is to plot $L^{-1}I$, which should correspond to the function $F(\alpha)$.

$$F(\alpha) = L^{-1}(i,\epsilon)I(i,\epsilon,\alpha) \qquad (2)$$

If the factorization is valid, the data on individual features should be symmetric about $\alpha = 0$.

$$F(-\alpha) = F(\alpha) \qquad (3)$$

Light from the whole moon should not be expected to be symmetric in positive and negative phases because of the larger area of maria at positive phases. Nevertheless, the assumption of factorizability as in (2) for each lunar area permits the separation of the total light $T(\alpha)$ as follows:

$$T(\alpha) = \left[1-\sin\frac{\alpha}{2}\tan\frac{\alpha}{2}\ln\cot\frac{|\alpha|}{4}\right] \times \bar{F}(\alpha) \qquad (4)$$

After inversion of (4), the transformed data on the whole moon corresponding to $\bar{F}(\alpha)$ should agree with the $F(\alpha)$ of an average individual lunar features, provided that it is valid to factor $I(i,\epsilon,\alpha)$ as suggested by Hapke. In fact, the lunar photometric data treated in this way show that factoring out a Lommel-Seeliger dependence is a very good approximation.

2. The Brightness of Selected Lunar Features

In Figs. 3-13, the data of GCO on the brightness in green light of 11 lunar features are presented as a function of phase angle. Negative phase angle data are indicated by circled points. Measurements that were considered less certain in GCO are indicated by crosses. One notices that in this range of phase angles one finds no decided tendency for the circled points to deviate from the other points. The curves drawn in Figs. 3-13 are for later reference. Historically, the rise of the data points above the reference curve at phase angle $|\alpha| < 10°$ had not been identified as real by any previous lunar investigators.

A few remarks are needed on the data comprising Figs. 3-13. The measurements were obtained with 4 different instruments, mostly at Goethe Link Observatory in Indiana with an angular aperture later determined to be about 13 sec of arc and at the Catalina instrument north of Tucson, Arizona, with an angular aperture of nearly 23". Photometric data on only three nights, all of questionable seeing, were reported from the U. S. Naval Observatory at Flagstaff, Arizona. The Flagstaff aperture was known to be 4.6" and the data from just one night at that instrument (near +12.1° phase) were fitted to those from Indiana. The choice appears to have been a poor one because, after removal of the Lommel-Seeliger dependence as in Figs. 3-13, the Flagstaff data from the other two phases (near -14° and $\pm$1°) are uniformly higher than the Indiana data. Therefore, we have multiplied all the Flagstaff data by a factor of 0.90. A few data were obtained, apparently with considerable experimental difficulty, at the McDonald Observatory near Fort Davis, Texas. The aperture was 5.02" and the data seem to have been fitted satisfactorily to the Indiana data.

It is necessary to give a detailed statement concerning the photometric data because it was suggested in GCO that an experimentally significant decrease in the brightness of these 11 features took place from 1956-59 to 1963-64. Solar activity also decreased in that period. Therefore the conjecture was entertained that a general luminescence of the moon might have been detected.

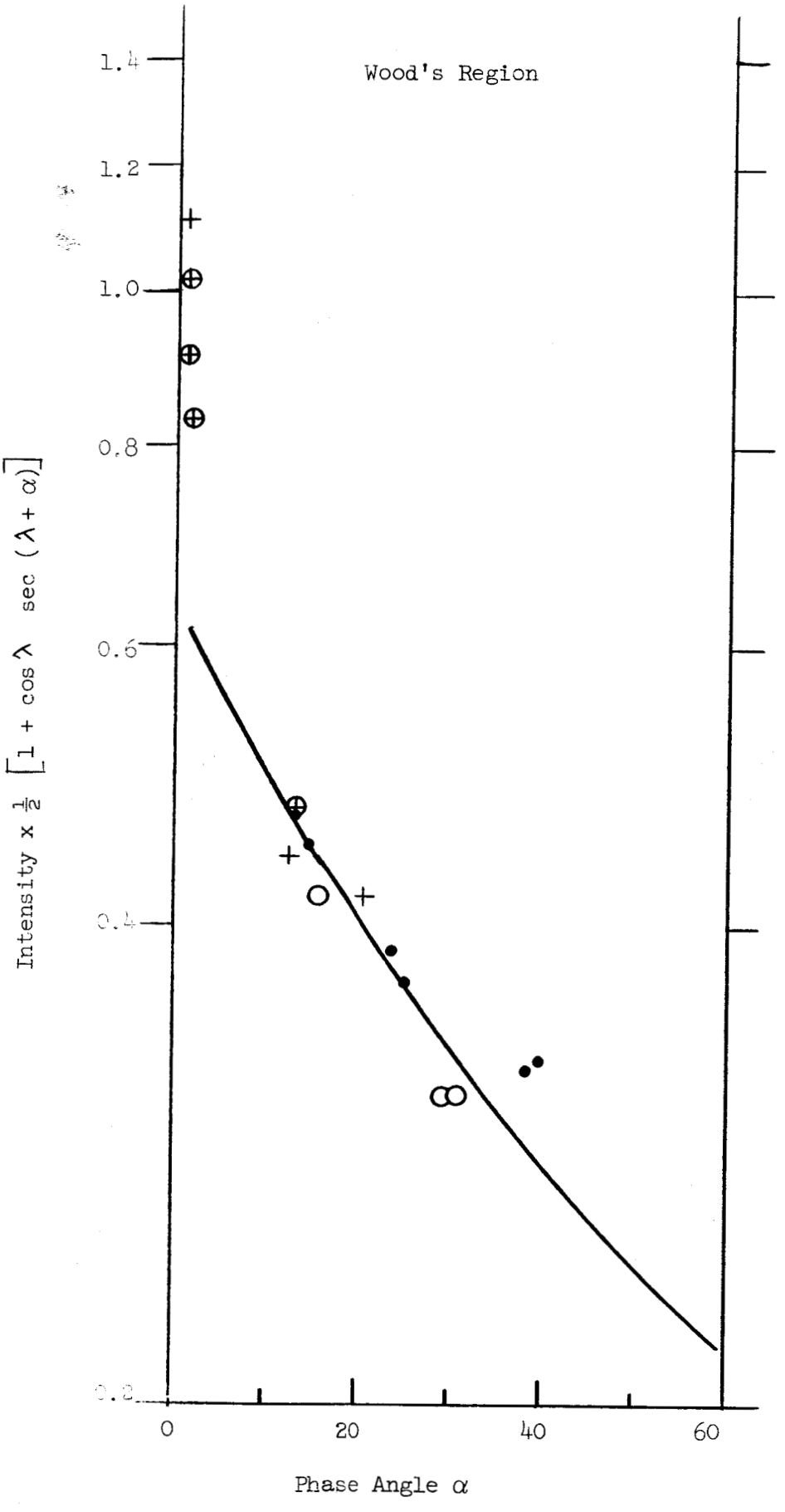

Fig. 3 F(α) for Wood's Region.

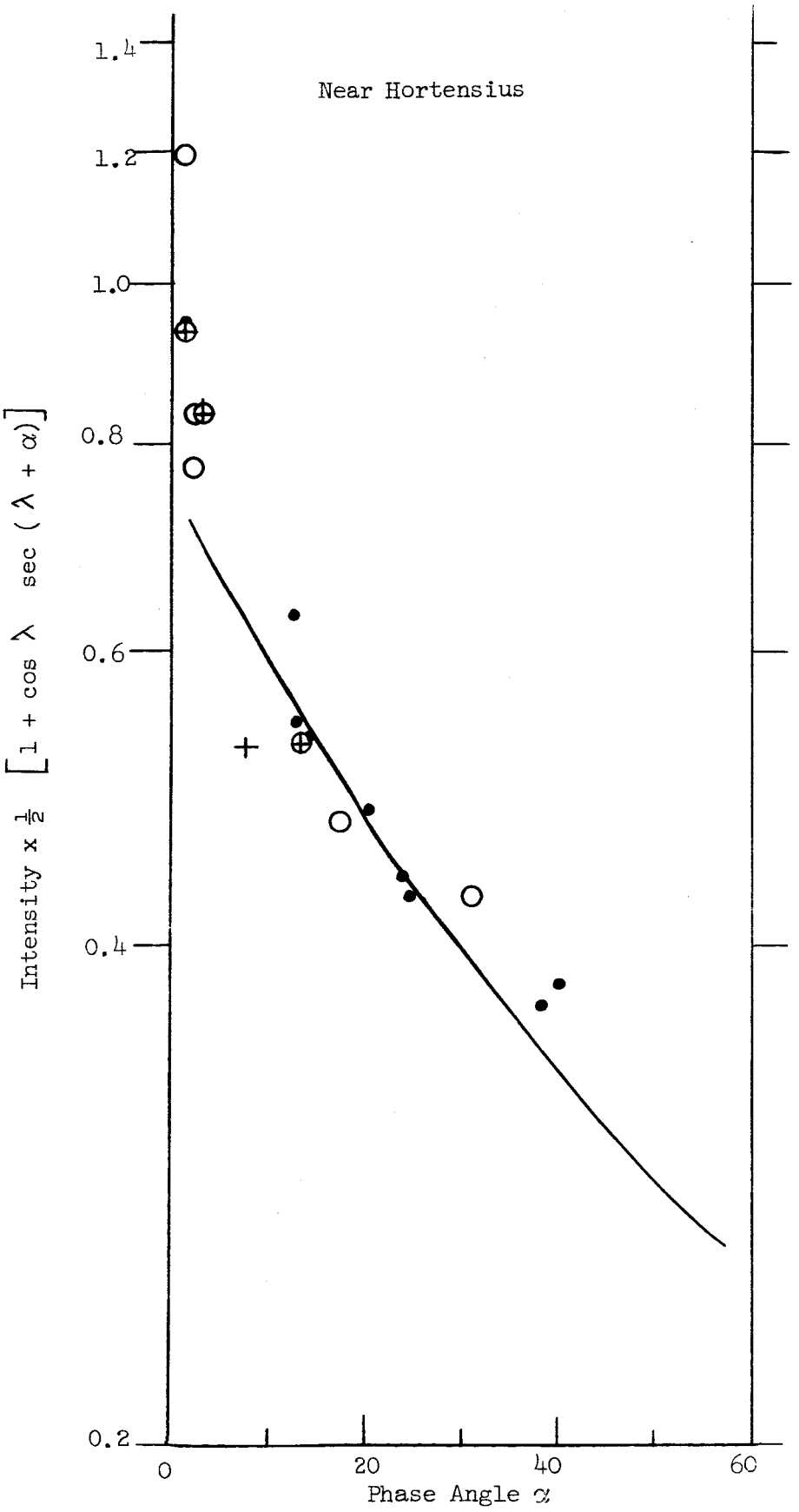

Fig. 4 F(α) Near Hortensius.

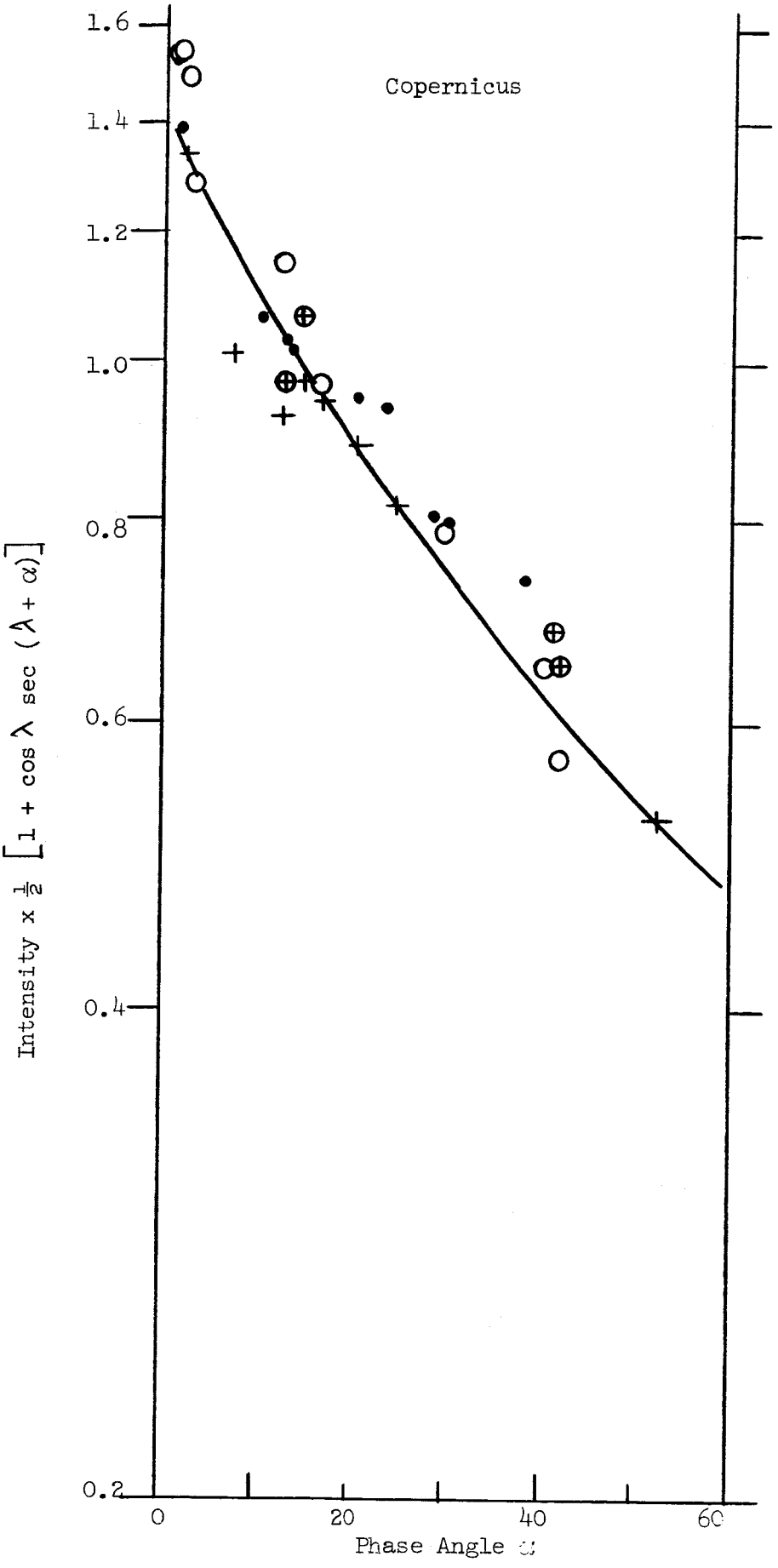

Fig. 5 F(α) for Copernicus.

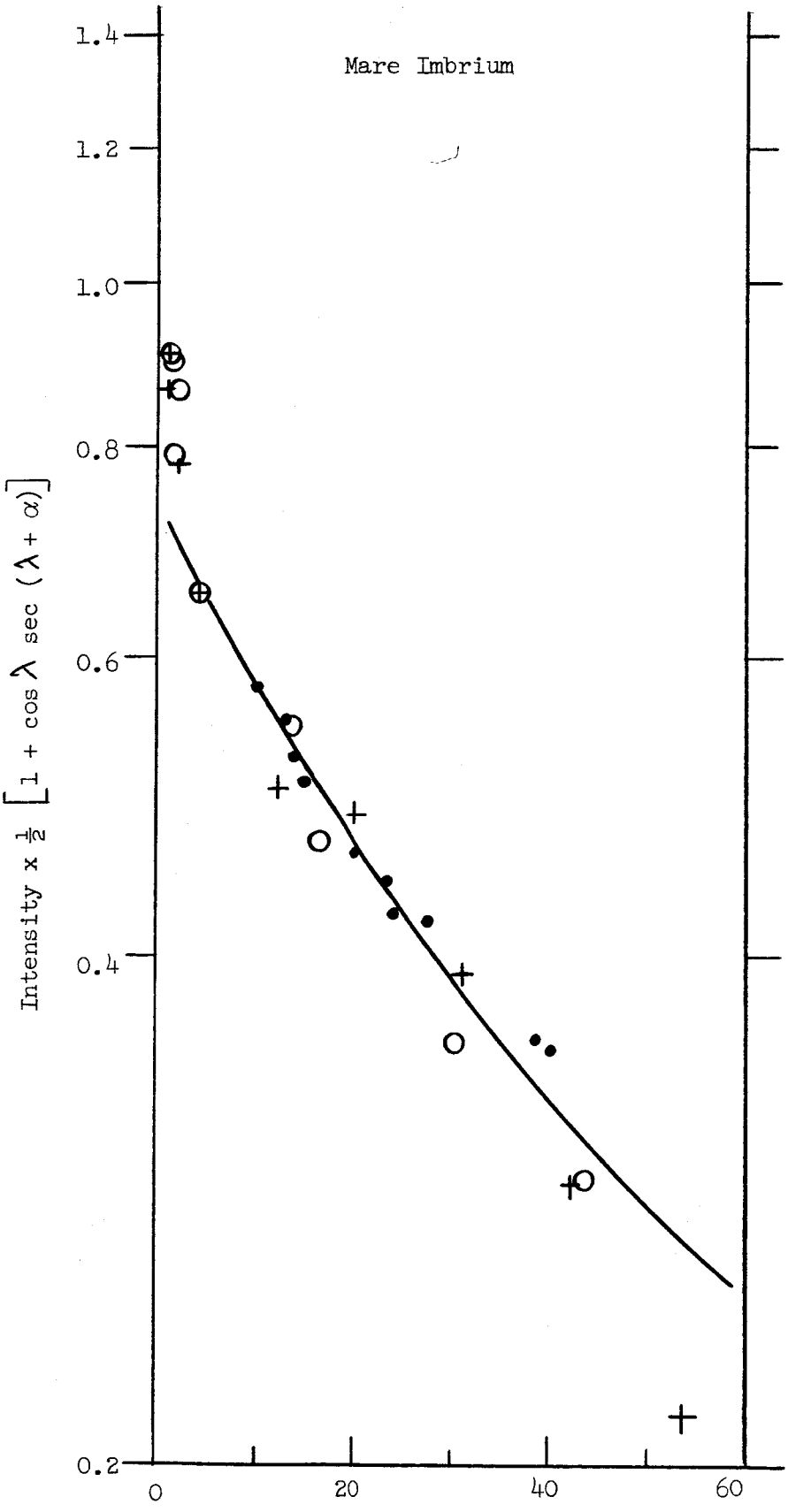

Fig. 6 F(α) for Mare Imbrium.

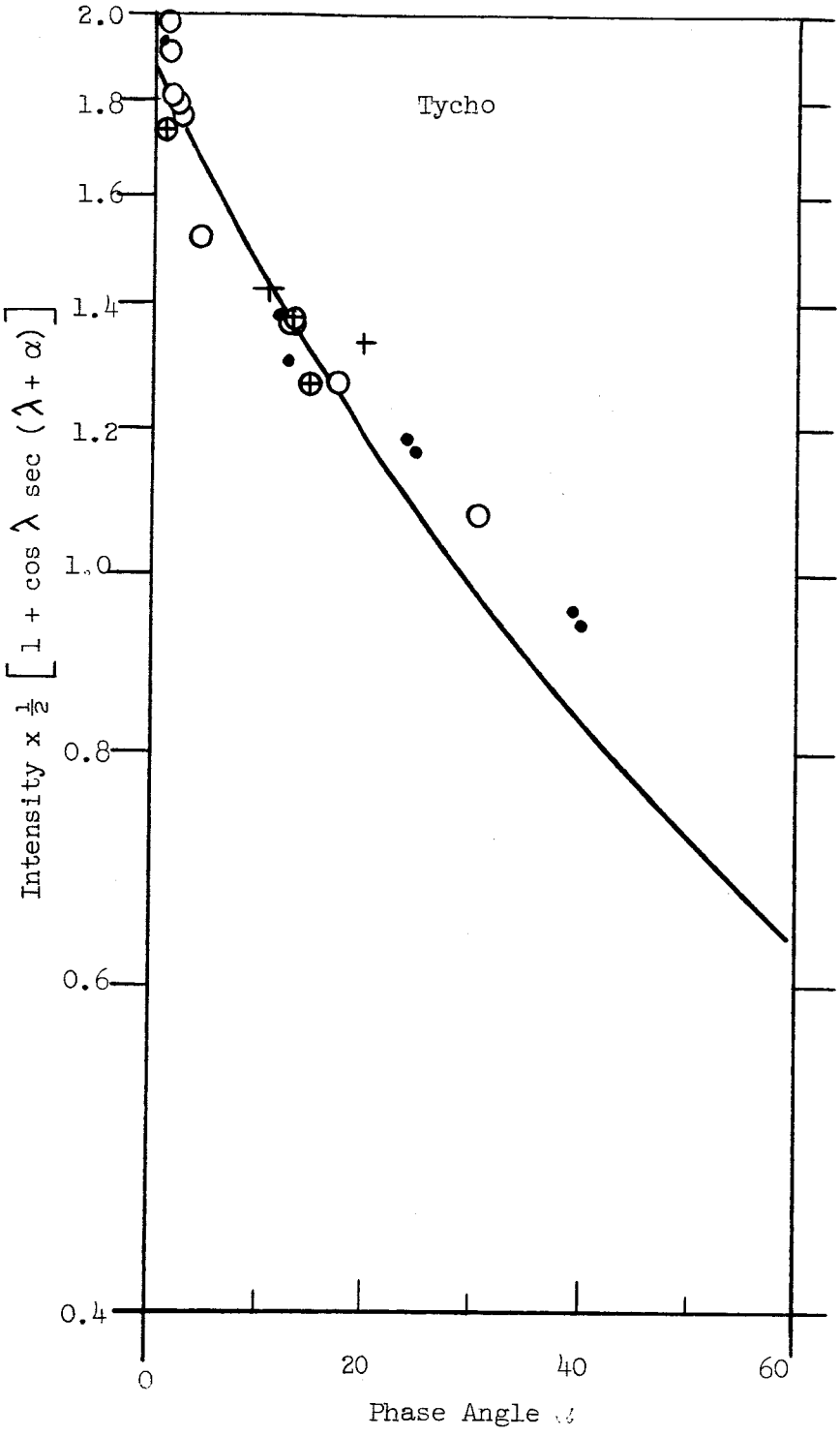

Fig. 7 $F(\alpha)$ for Tycho.

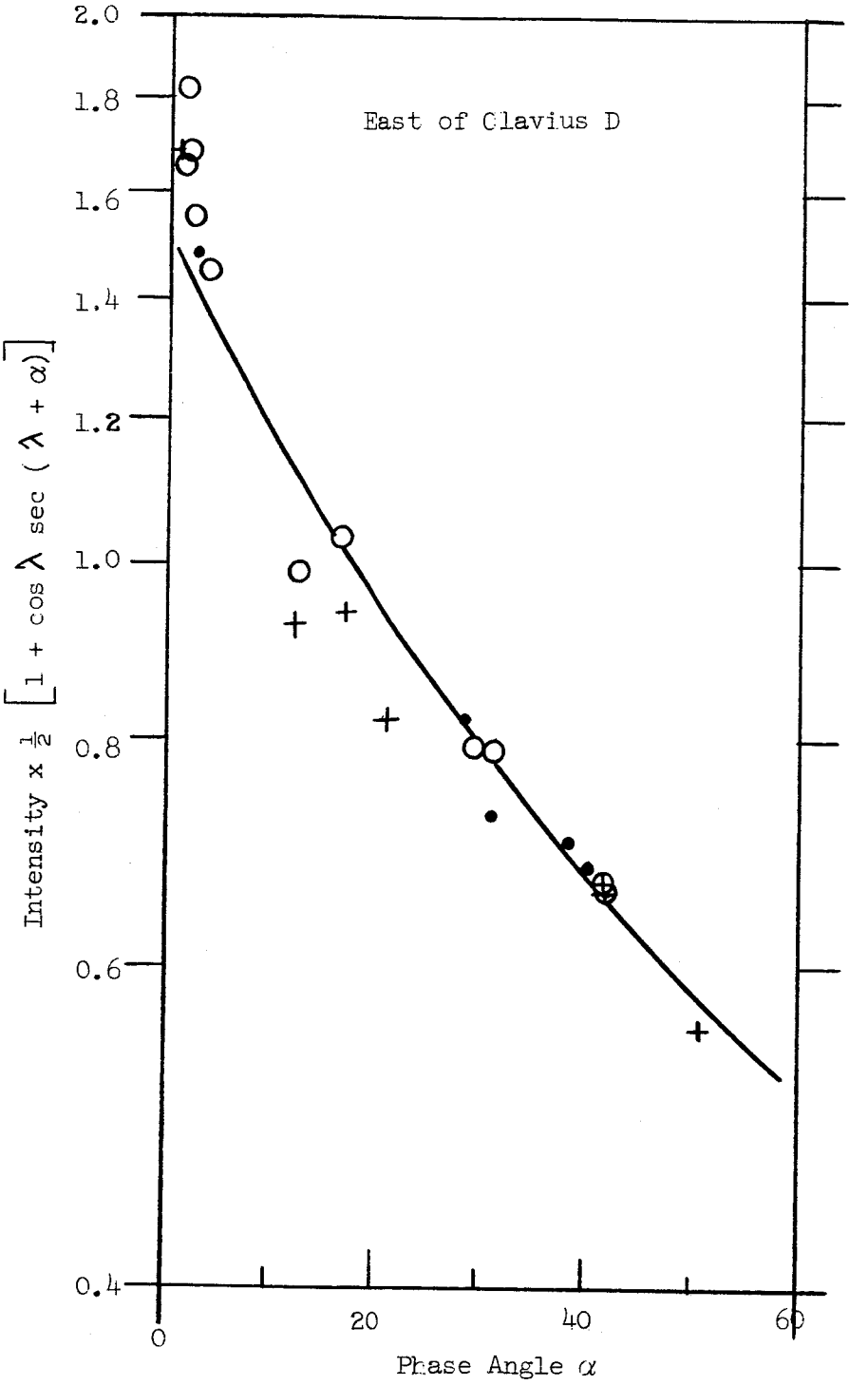

Fig. 8 F(α) for East of Clavius D.

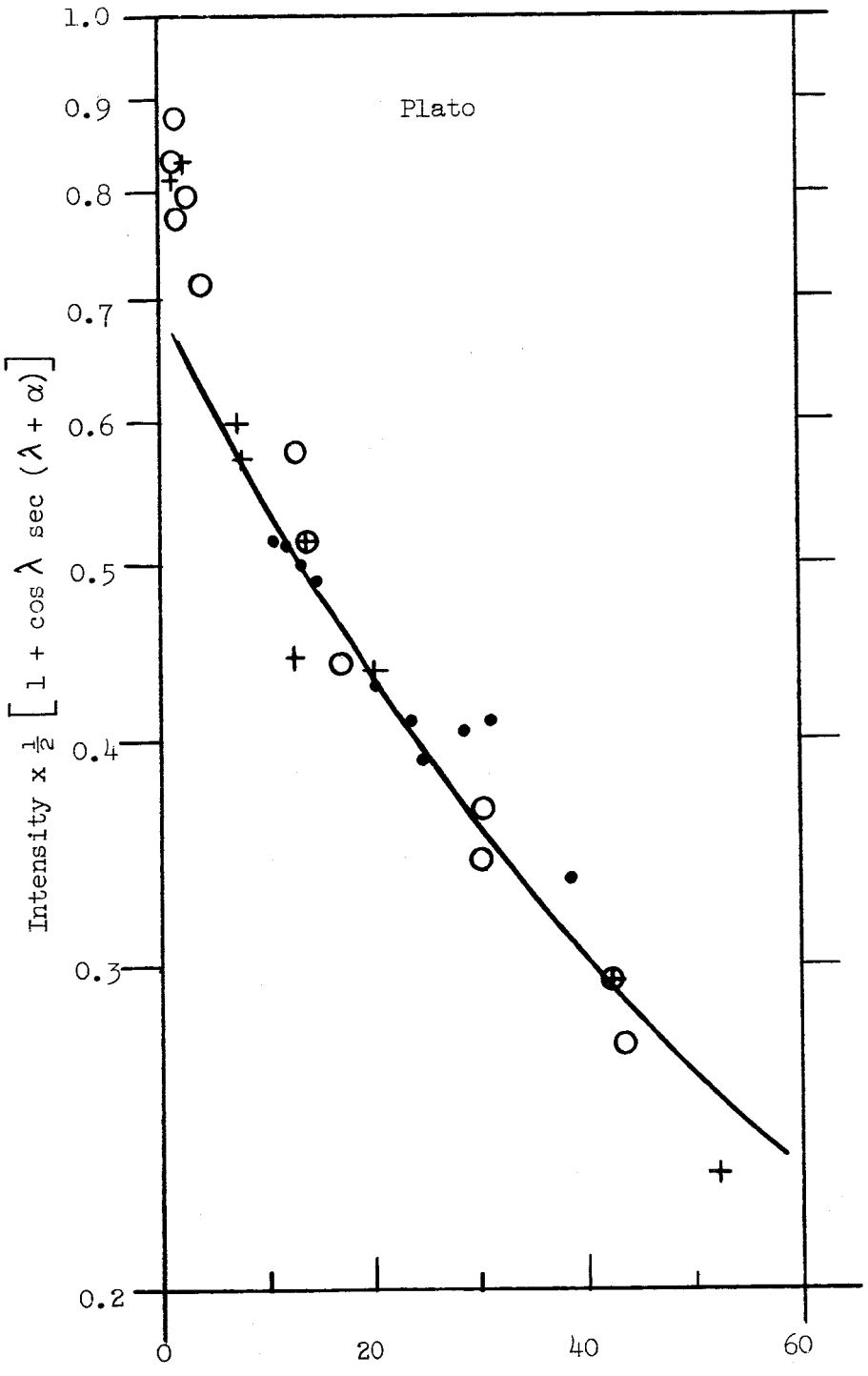

Fig. 9 F(α) for Plato

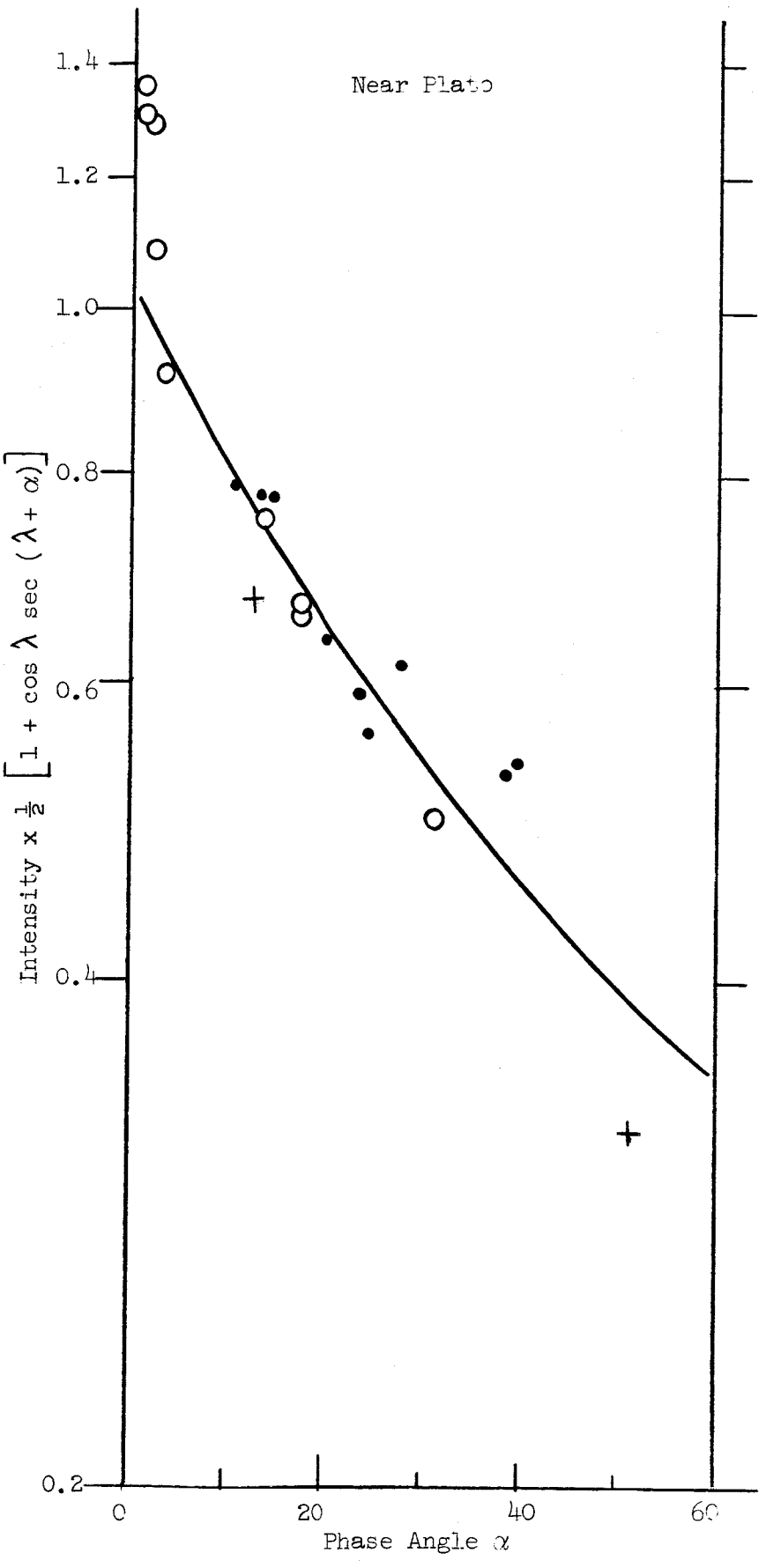

Fig. 10 F(α) Near Plato

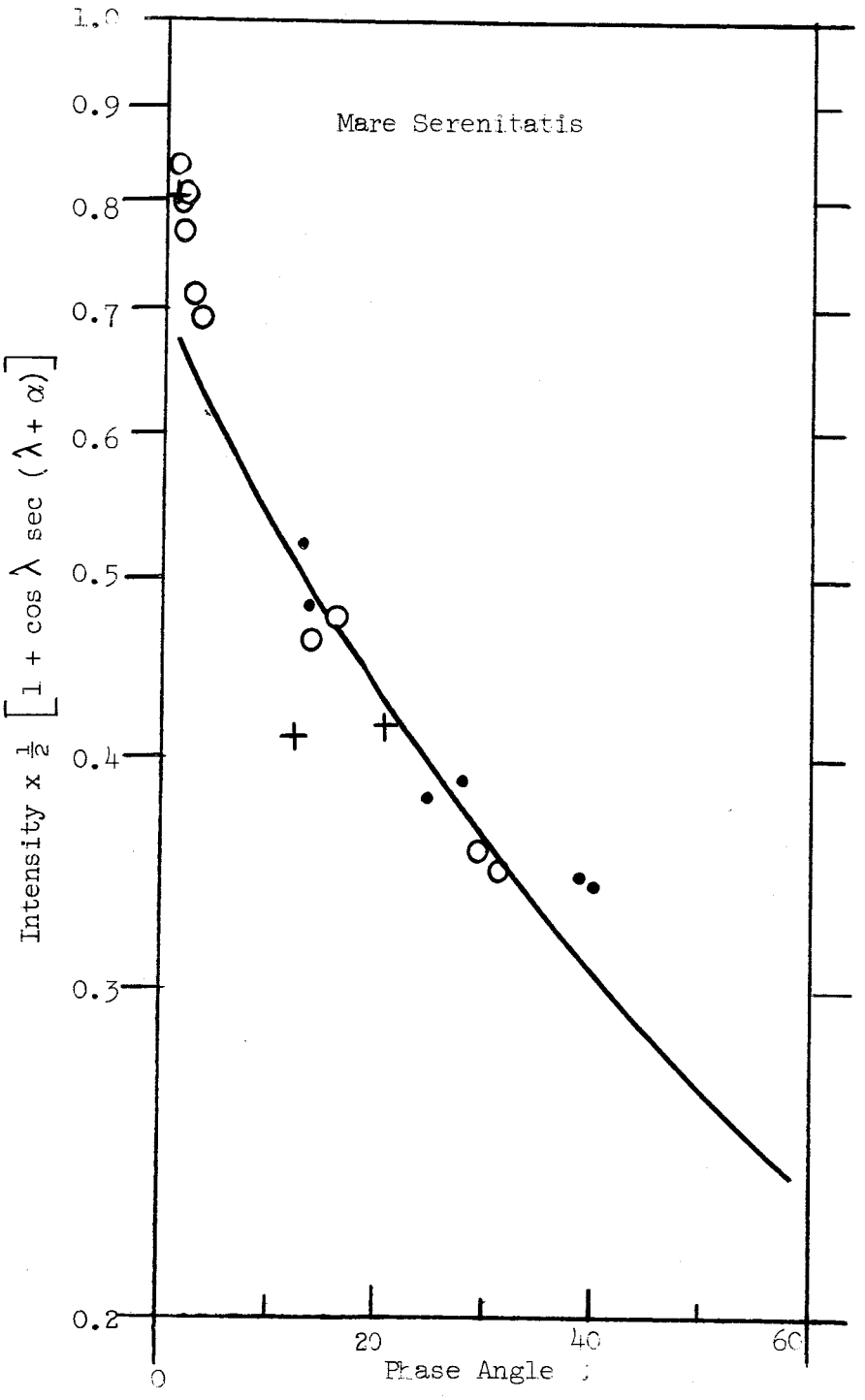

Fig. 11 F(α) for Mare Serenitatis

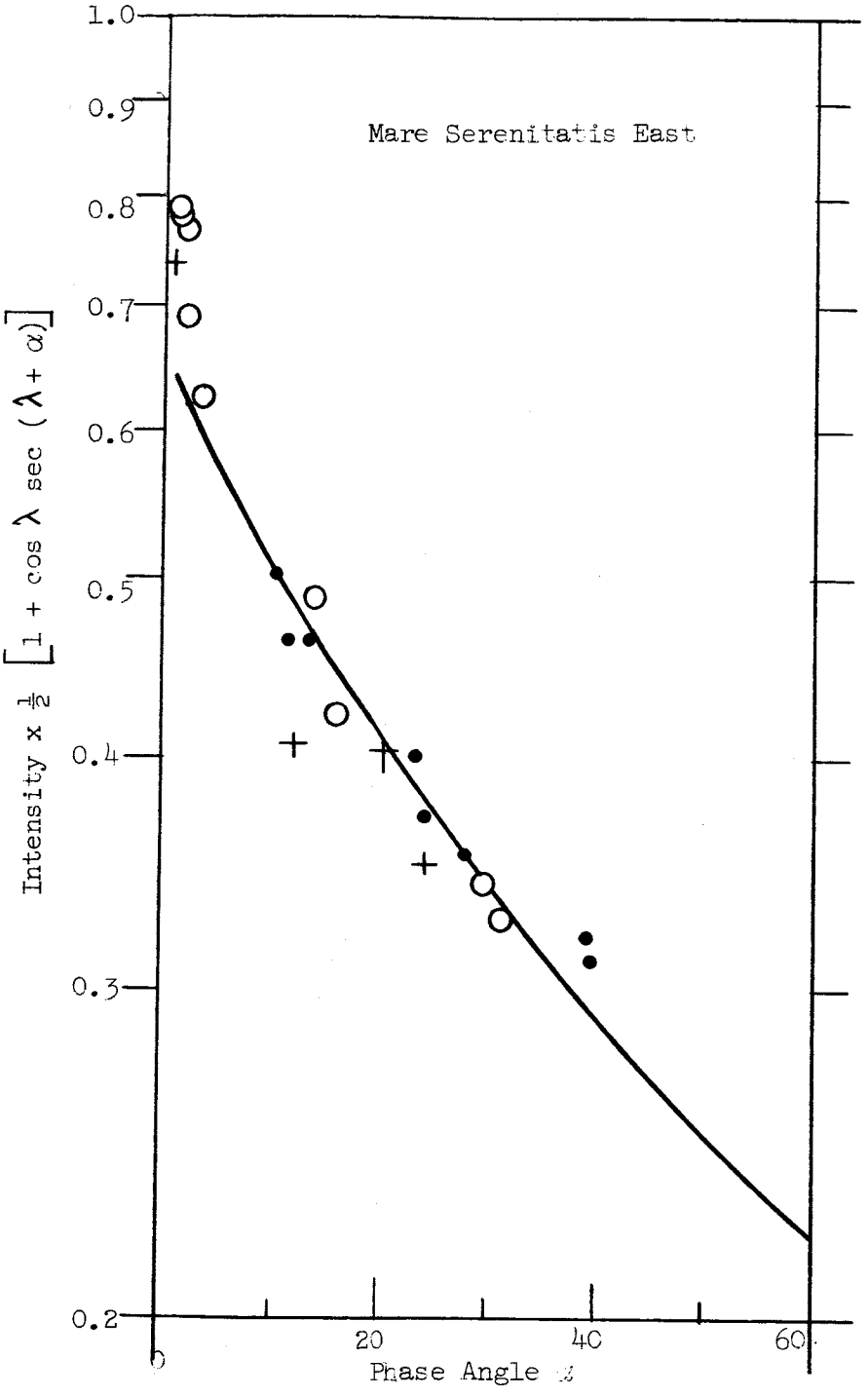

Fig. 12 F(α) for Mare Serenitatis East

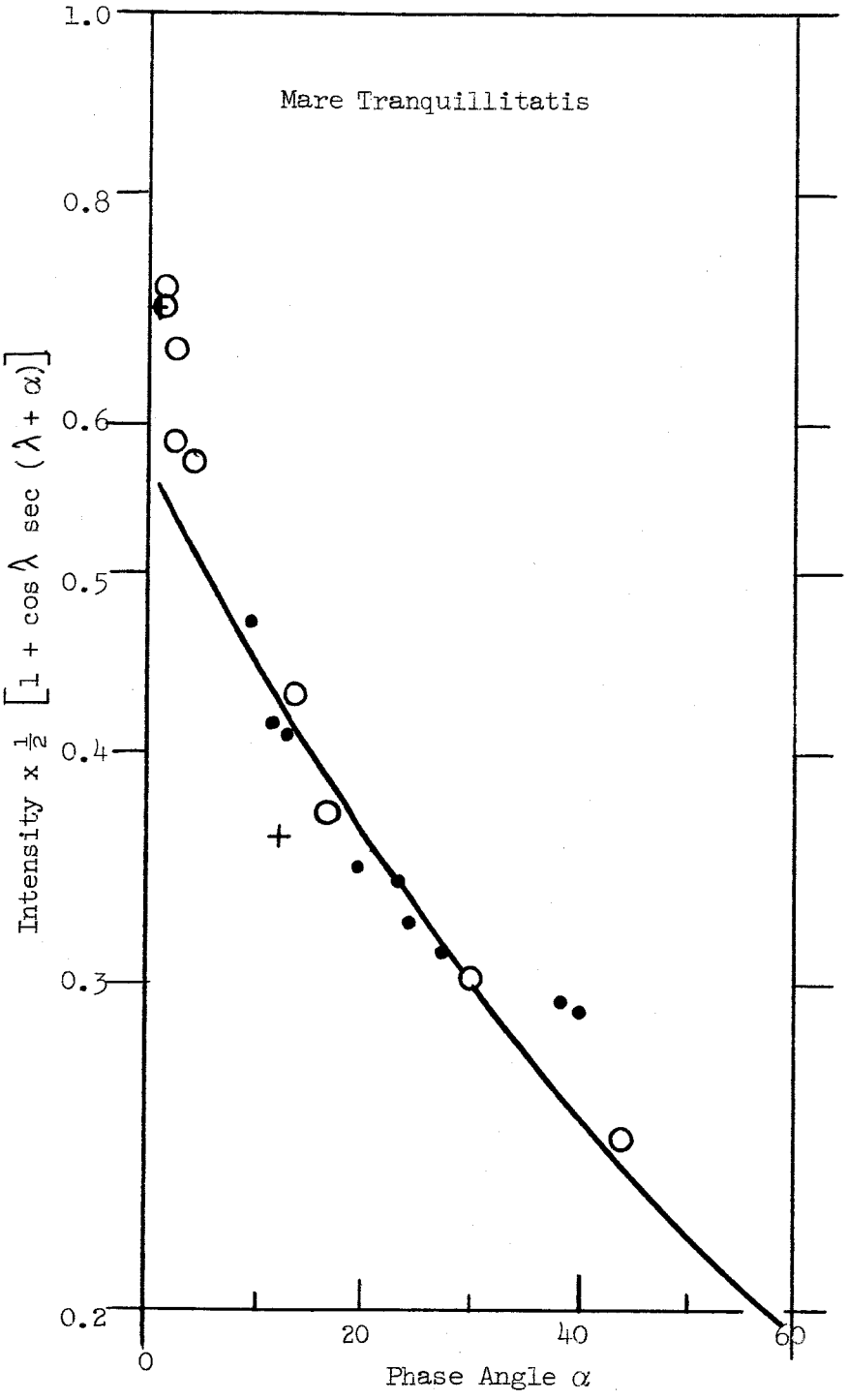

Fig. 13 F(α) for Mare Tranquillitatis

Because of this suggestion, we plotted the Catalina data (1963-64) separately from the other data (1956-59). Positive and negative phase data were kept separate. The bulk of the Catalina data are for negative phases (before full moon). This was a deliberate choice on the part of the observer in order to correct for a predominance of positive phases in the earlier data. Without any assumption except smoothness about the shape of $F(\alpha)$, we tried to determine the "decrease" factors that should multiply the earlier data for each of the 11 features so as to bring them into agreement with the Catalina data. Because we did not want to influence the test as to whether $F(-\alpha) = F(\alpha)$ in Figs. 3-13, we determined the "decrease" factor for each feature by superimposing the two plots for each feature either with phase angle increasing in the same sense in the two plots or with phase angles reversed. In the latter case, the abundant data of Catalina at negative phases was superimposed on the abundant earlier data of positive phases. If the "decrease" factors had been significantly different in the former and latter cases, then the test of $F(-\alpha) = F(\alpha)$ would not be reliable in Figs. 3-13. With phases in the same sense, the "decrease" factor averaged 0.87 with a scatter of about ± 0.03. With phases in reversed sense, the "decrease" factor averaged 0.86. The scatter in the latter determinations was, of course, markedly less: about ± 0.01. We conclude that the "decrease" factor was independent of the phase angle reversed. The feature Tycho had a significantly different "decrease" factor. The data required a brightness "decrease" of 0.81 for either sense of the phases for Tycho. This greater decrease for Tycho is probably due to the larger angular aperture of the

Catalina instrument: a 23" aperture certainly includes some of the darker area surrounding Tycho. In plotting Figs. 3-13, all the Catalina data were increased by $(0.86)^{-1}$ except for Tycho, where the increase was $(0.81)^{-1}$. All these data are given in Tables I and II. In Table I the Flagstaff intensities are all reduced by 0.90. The Catalina intensities have not been increased in Table II but are given as in GCO. In addition, the intensities of 8 additional features are given. These features were measured at only a few phases but the data should permit the assignment of relative brightnesses to these additional features.

By a completely different procedure in GCO, it was suggested that the decrease in lunar brightness from 1956-59 to 1963-64 was 10 to 20% and probably not less than 14%. Since it is actually the Flagstaff data from 3 nights of questionable seeing that are being compared to the Catalina data ("known" apertures), our analysis implies a "decrease" of (0.90) x (0.86) = 0.774 in the brightness of 10 lunar features. Since the colors of these features did not change in this period, the indicated "luminescence" is distributed evenly throughout the optical spectrum and is not less than (100-77.4)/77.4 = 0.29 as intense as reflected sunlight. Since luminescent efficiencies are commonly a few percent or less, there simply is no conceivable energy source for "luminescence" of this magnitude. Surely uncertainties in instrument intercalibrations of the order of 10% are a more reasonable explanation of the intensity shifts.

Table I - Removal of Lommel-Seeliger dependence from brightnesses of 19 lunar features studied in GCO[16] during 1956-59.
$F = 10^{-0.4\,V} \times \frac{1}{2}\left[1 + \cos\lambda \sec(\lambda + \alpha)\right]$.

α (deg.)	$F(\alpha)$	α	$F(\alpha)$
Wood's Region $(\lambda,\beta) = (-51°17', 29°15')$		M. Humorum $(-42°37', -22°28')$	
-13.1 f[a]	0.475:	1.6 m	0.742
- 1.7	0.832:	2.1 m	0.694:[b]
- 1.3 f	1.021:	16.3 m	0.440[c]
- 1.1	0.914:	31.5 m	0.348
0.9 f	1.111:	Near Hortensius $(-29°21', 07°20')$	
12.2 f	0.443:	-13.2 f	0.529:
12.9	0.468	- 2.0	0.833
14.4	0.450	- 1.2 f	1.193
20.6	0.418:	- 1.2	0.934:
23.9	0.386	0.9 f	0.947
24.9	0.368	7.7 m	0.528
69.4	0.0978:	12.2	0.630
Aristarchus $(-47°22', 23°35')$		12.7	0.544
-13.6 f	1.503	14.1	0.533
12.4 f	1.512:	20.3	0.482
53.2 m	0.698	23.8	0.440
		24.5	0.428

(a) Data at unmarked phases from Indiana. Data marked "f" from Flagstaff, "m" from McDonald.

(b) "Correction includes presumed tube voltage change."

(c) "Hazy, poor calibration."

(d) "Poor seeing."

The colon indicates data considered particularly uncertain in GCO.

Table I (Cont'd.)

α	$F(\alpha)$
Near Copernicus (-23°25', 09°42')	
-41.9 m	0.504:
-41.4 m	0.498:
1.6 m	1.152
16.5 m	0.704[c]
30.5 m	0.574
Copernicus (-20°08', 10°11')	
-42.0 m	0.626:
-41.4 m	0.642:
-14.4 f	1.066:
-12.8 f	0.971:
-12.4	1.148
- 2.2	1.496
- 1.6	1.550
- 1.4 f	1.543
0.8 f	1.530
1.5 m	1.386
2.1 m	1.338:[b]
7.1 m	1.010:[d]
10.1	1.062
12.1 f	0.927:
12.5	1.030
13.2	1.018
14.7	0.972:

Cont'd. in Second Column

α	$F(\alpha)$
Copernicus (Cont'd.)	
16.4 m	0.944[c]
20.2	0.952
20.5 m	0.888:[d]
23.5	0.936
24.5	0.816:
30.4 m	0.798
52.5 m	0.524:
Mare Imbrium (-17°44', 46°08')	
-42.2 m	0.294:
-13.7 f	0.549
- 2.1	0.868
- 1.6	0.900
- 1.4 f	0.912:
1.0 f	0.866:
2.0 m	0.782:[b]
10.1	0.576
12.2 f	0.502:
12.5	0.552
13.5	0.526
14.8	0.508
20.2	0.460
20.2 m	0.486:[d]
23.7	0.444
24.2	0.424
31.1	0.390
53.4	0.215

Table I (Cont'd.)

α	F(α)
Tycho (-11°17', -43°18')	
-14.6 f	1.264:
-13.4 f	1.377
-12.8 f	1.373
-12.7	1.380
- 2.5	1.762
- 1.4 f	1.904
- 1.2 f	1.735:
- 1.1	1.982
1.0 f	1.930
10.5	1.428:
11.6	1.380
12.2	1.300
13.3	1.380:
19.6	1.336:
23.5	1.182
24.1	1.162
East of Clavius D (-10°03', -58°41')	
-42.1 m	0.660:
-41.6 m	0.668:
-12.7 f	0.992
- 1.7	1.824
- 1.4 f	1.656
0.8 f	1.683:

Cont'd. in Second Column

α	F(α)
East of Clavius D (Cont'd.)	
2.4 m	1.480
12.1 f	0.927:
16.8 m	0.940[c]
21.0 m	0.822:[d]
31.1 m	0.728
52.8 m	0.556:
Plato, W of Center (-10°32', 51°25')	
-42.4 m	0.296:
2.0 m	0.830:[b]
7.2 m	0.598:[d]
7.7 m	0.572
20.3 m	0.474:[d]
31.0 m	0.412
52.2 m	0.232
Plato, Center (-09°18', 51°28')	
-13.8 f	0.517:
-12.5	0.578
- 2.6	0.798
- 1.5	0.880
- 1.3 f	0.837
1.0 f	0.814:
10.3	0.516
11.5	0.512

Cont'd. on Following Page

Table I (Cont'd.)

α	F(α)
Plato, Center (Cont'd.)	
12.2 f	0.445:
13.1	0.500
14.4	0.490
19.9	0.428
23.3	0.410
24.2	0.390
Plato, E of Center (08°16', 51°46')	
69.7	0.0528:
82.2	0.0600:[d]
Near Plato (-07°10', 54°36')	
-13.7 f	0.751
- 2.1	1.286
- 1.3	1.358
- 1.2 f	1.303
1.0 f	1.303:
10.4	0.792
12.2 f	0.675:
13.1	0.778
14.5	0.773
20.0	0.618
23.5	0.596
24.3	0.580
53.3 m	0.326
M. Serenitatis (21°59', 25°03')	
-13.9 f	0.464
- 1.8	0.812
- 1.4 f	0.794
- 1.3	0.836
0.9 f	0.801:
12.0 f	0.412:
12.5	0.524
13.4	0.484
20.4	0.418:
24.5	0.382
Nicolai (25°59', -42°23')	
18.3 m	1.058
M. Serenitatis, E (26°50', 28°02')	
-13.9 f	0.488
- 2.1	0.766
- 1.4 f	0.779
- 1.3	0.790
0.9 f	0.738
10.4	0.502
11.6	0.462
12.0 f	0.407
13.3	0.464
20.3	0.404:

Cont'd. on Following Page

Table I (Cont'd.)

α	$F(\alpha)$
M. Serenitatis, E (Cont'd.)	
23.5	0.400
24.2	0.372
24.4	0.352:
52.9 m	0.848
M. Tranquilitatis (39°10', 11°34')	
-13.6 f	0.430
- 2.6	0.662
- 1.6	0.716
- 1.5 f	0.695
0.9 f	0.695:
9.7	0.472
11.5	0.414
12.1 f	0.360:
13.0	0.408
19.5	0.346
23.3	0.340
24.1	0.324
Palus Somni (45°36', 12°41')	
20.9	0.584[d]
Mare Crisium (52°43', 17°18')	
-42.5	0.298:
-41.9	0.302:
1.5	0.862
16.5	0.448[c]
21.0	0.384[d]
30.4	0.361

Table II - Removal of Lommel-Seeliger dependence from brightnesses of 13 lunar features studied in GCO(16) during 1963-64.

$F = 10^{-0.4\,V} \times \frac{1}{2}\left[1 + \cos\lambda \sec(\lambda + \alpha)\right]$.

α	$F(\alpha)$
Wood's Region (-50°00', 28°00') = (λ,β)	
-30.9	0.269
-29.3	0.268
-15.9	0.359
- 3.6	0.595
- 2.0	0.628
38.0	0.279
39.7	0.284
Mare Humorum (-40°38', -21°40')	
-44.0	0.282
-30.1	0.259
-29.4	0.269
-17.0	0.339
- 4.5	0.486
- 1.8	0.599
27.6	0.294
38.5	0.255
39.9	0.248

α	$F(\alpha)$
Near Hortensius (-29°22', 07°17')	
-31.1	0.368
-17.2	0.409
- 3.2	0.717:
- 2.2	0.664
38.1	0.317
39.7	0.327
Copernicus (-20°08', 10°11')	
-44.2	0.560:
-29.9	0.678
-16.3	0.837
- 3.2	1.108
- 2.2	1.149
28.1	0.691
38.1	0.634
Mare Imbrium (-17°37', 46°13')	
-43.7	0.254
-30.5	0.306
-16.6	0.402
- 4.4	0.564:
- 1.9	0.681

Cont'd. on Following Page

Table II (Cont'd.)

α	$F(\alpha)$
Mare Imbrium (Cont'd.)	
27.7	0.360
38.5	0.307
40.1	0.302
Tycho (-11°17', -43°18')	
-30.6	0.872
-17.0	1.030
- 4.3	1.230
- 2.0	1.453
- 1.8	1.468
27.5	0.897
39.1	0.776
39.9	0.762
E of Clavius D (-10°00', -58°24')	
-31.3	0.680
-29.2	0.681
-16.5	0.892
- 4.0	1.247
- 2.2	1.335
- 1.9	1.448
28.2	0.708
38.2	0.606
40.1	0.587
Plato, Center (-09°18', 51°28')	
-43.6	0.235
-30.1	0.297
-30.1	0.317
-17.1	0.380
- 4.1	0.614
- 1.8	0.665
28.0	0.348
38.3	0.289
Near Plato (-07°50', 55°09')	
-31.2	0.431
-17.4	0.576
-17.4	0.567
- 3.5	0.787
- 2.4	0.933
27.9	0.529
38.3	0.457
39.5	0.464
Mare Serenitatis (21°36', 25°30')	
-31.5	0.300
-29.8	0.306
-16.2	0.409
- 3.7	0.593

Cont'd. on Following Page

Table II (Cont'd)

α	$F(\alpha)$
Mare Serenitatis (Cont'd)	
- 2.5	0.616
- 1.8	0.661
27.7	0.335
38.4	0.297
39.7	0.294
M. Serenitatis, E (28°06', 28°38')	
-31.6	0.283
-29.9	0.295
-16.0	0.364
- 3.8	0.539
- 2.2	0.595
28.0	0.305
39.0	0.276
39.7	0.268
M. Tranquillitatis (39°17', 11°45')	
-44.1	0.213
-30.0	0.260
-16.8	0.318
- 4.3	0.495
- 2.7	0.508
27.2	0.269
38.2	0.252
40.0	0.248

α	$F(\alpha)$
Mare Crisium (53°14', 17°23')	
-45.2	0.274
-30.8	0.346
-17.3	0.422
- 4.7	0.587:
- 1.8	0.722
27.1	0.396
27.5	0.501:
37.6	none[a]
39.2	none[a]

(a) Indicated area beyond terminator, data reported for incorrect area.

Adopting the position, then, that the data of Figs. 3-13 have been reduced to a homogeneous basis, we note the following features about $F(\alpha)$ and this procedure.

(1) The test that $F(-\alpha) = F(\alpha)$ (i.e., that multiplication of intensities of lunar features by $L^{-1}(i,\epsilon) = 1 + \cos\epsilon \sec i$ completely removes dependence on angles of incidence and emergence) is, of course, most stringent for features away from the central lunar meridian. In Wood's Region (Fig. 3), for example, the points near $|\alpha| = 30°$ compare angles of incidence near 80° (negative phase) to incidence near 20°. If there were a systematic residual dependence on angle of incidence in Figs. 3-13, then the features having negative longitude (Wood's region) might have the intensities from negative phase angles systematically lower than the intensities from positive phases. But the features of positive longitude (Mare Tranquillitatis) would have to exhibit the opposite systematic tendency. No such systematic shifts are found in Figs. 3-13, which are ordered according to longitude.

(2) The uncertainty in $F(\alpha)$ for each feature in the interval $1° < |\alpha| < 40°$ is probably less than 5%. This means that relative brightnesses of 5% precision can be determined for these features. Since the shape of $F(\alpha)$ does not vary greatly in Figs. 3-13 for $|\alpha| \gtrsim 10°$ and since we have shown that $F(-\alpha) = F(\alpha)$, we point out that the determination of relative brightnesses is greatly facilitatedby the removal of the Lommel-Seeliger dependence from lunar photometric data.

(3) It is clear from Figs. 3-13 that the shape of $F(\alpha)$ hardly varies for the 11 lunar features. In each figure a reference curve is drawn for the reader's convenience. It is taken from Fig. 14 where data for the whole moon will be studied. The reference curve follows the general trend of measurements for $|\alpha| > 10°$ for all the features except Tycho (Fig. 7). The brightness of the ray crater Tycho definitely does not decrease as rapidly with increasing $|\alpha|$ as does the reference curve. Besides this photometric anomaly, Tycho is an anomalously bright radar scatterer, has an anomalously long time constant in temperature changes, and exhibits anomalously small difference in the backscatter of radar having linear polarization in, or perpendicular to, the plane of incidence. All these evidences point to a thinner, less tenuous surface layer within Tycho. Exposed rocks are probably more numerous there than in general.

(4) Near $\alpha = 0$ the shape of the function $F(\alpha)$ is so very uncertain for all the features that extrapolation of the measurements to $\alpha = 0$ is doubtful. In particular, it seems doubtful that any differences in the shape of $F(\alpha)$ for $|\alpha| < 10°$ can be asserted on the basis of these data. At most, there might be a tendency near $\alpha = 0$ for the rise of $F(\alpha)$ above the reference curve to be slightly less for the brightest of the 11 features: Tycho, Clavius, and Copernicus in decreasing order of brightness. The reason that the shape of $F(\alpha)$ near $\alpha = 0$ is so important is that the shape is presumably governed by the structure of the surface layer covering the feature. Only the brightness at $\alpha = 0$ can be expected to be free from the effect of shadows in the surface layer. Therefore in laboratory

simulation of the lunar surface layer, only the sample brightness at $\alpha = 0$ can be unambiguously matched to the lunar brightness. At any other phase angle, discrepancy between the sample structure and the lunar surface structure affects the results to some degree.

3. The Brightness of the Whole Moon

The brightness of the whole moon $T(\alpha)$ was carefully measured by Rougier[18] in 1928-32. If the moon is assumed to have a spherical, homogeneous surface, then the Lommel-Seeliger contribution to $T(\alpha)$ is given in Eq. (4). After removal of the Lommel-Seeliger contribution, the data of Rougier for $|\alpha| < 60°$ was plotted in Fig. 14. Note that Rougier had to allow for atmospheric absorption by extrapolation to zero atmosphere. We follow his notation in indicating the number of brightness determinations entering that extrapolation by using, in Fig. 14, a circled point for 4-5 determinations (in half a night), a cross for 2-3 determinations, and a point for 1 determination (estimated atmospheric absorption). In his Table XXX (see also van Diggelen,[19] Ch. 2) Rougier suggested a fitted curve for $T(\alpha)$ at 5° intervals. His curve becomes the solid curve in Fig. 14, except that we drew a linear curve near $\alpha = 0$. It is Rougier's curve for positive phase angles that is drawn in Figs. 3-13.

Note that the data of Rougier tend to lie above his suggested curve at phase angles $|\alpha| < 10°$. Therefore the whole-moon data of Rougier at small phase angles confirm the non-linear brightness increase found at small phase angles in GCO. In particular, the behavior of the brightness

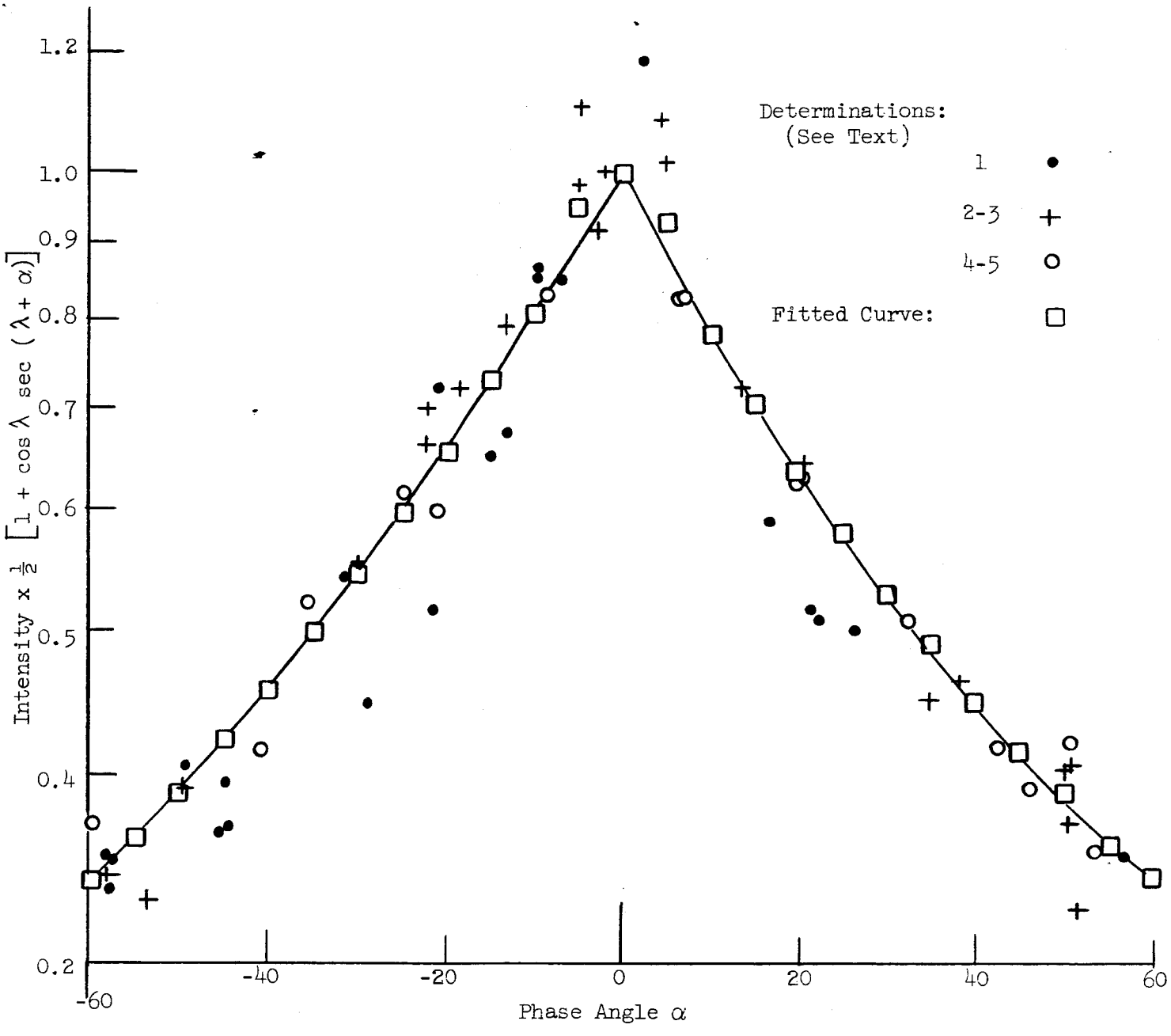

Fig. 14 Brightness of the whole moon after Rougier.(3) The influence of varying angles of incidence and emergence has been removed by assuming this effect is governed by Lommel-Seeliger scattering.

at small phase angles described in GCO for 11 features is undoubtedly characteristic of the whole moon.

Since the right-hand solid curve in Fig. 14 ($\bar{F}(\alpha)$) is the reference curve in Figs. 3-13, the excellent agreement of $\bar{F}(\alpha)$ with $F(\alpha)$ for 10 of 11 features surely implies that the brightness of the moon's features is accurately approximated by the product $L(i,\epsilon)F(\alpha)$.

The brightness of the whole moon at zero phase angle was given by Rougier as $V_o = -12.83^m$. Upon consideration of two other such determinations, Harris[20] adopts $V_o = -12.74^m$. The extrapolation adopted in GCO yielded a brightness larger by a factor of 1.754, namely $V_o = -13.35^m$. Analysis of Figs. 3-13 shows that a factor as large as 1.754 is probably unwarranted as a correction to the photometric curve given by Rougier. Considering that the data for Tycho, Clavius, and Copernicus must be at least doubly weighted to correct for the small number of bright areas that are sampled in GCO, then the curve given by Rougier should be corrected upward by a factor not greater than 1.3 at zero phase angle.

The reason that the brightness of the full moon is important here is that, using $V_o = -12.74^m$ for the moon and $V = -26.81^m$ for the sun, Harris gives $p(V) = 0.115$ for the geometric albedo of the moon (brightness relative to a perfectly white Lambertian scatterer at zero phase angle). Without doubt the data in GCO imply that $p(V)$ must be revised upward. But if a large revision like 1.75 were required, then the interpretation of the darkening effects resulting from the solar wind will be appreciably changed. In particular, the inferred geometric albedo of 20.2% is comparable to that of many powders that have not been darkened at all. Our analysis suggests that $p(V) \simeq 15\%$ is a reasonable value.

C. Photometry of Some Samples Darkened by Hydrogen Ion Bombardment

1. Test of Lommel-Seeliger Scattering

The measurements of GCO include none that are reliable at phase angles larger than 60°. But because of the generally favorable indication in the previous section that the intensity of light scattered from lunar features is well represented by $I(i,\epsilon,\alpha) = L(i,\epsilon)F(\alpha)$, it seems reasonable to assume approximate validity of this relation at larger angles. Then the data of Rougier on the brightness of the whole moon $T(\alpha)$ may be transformed to

$$\bar{F}(\alpha) = T(\alpha)\left[1 - \sin\frac{\alpha}{2}\tan\frac{\alpha}{2}\ln\cot\frac{|\alpha|}{4}\right]^{-1} . \qquad (4a)$$

The curve Rougier fitted to his data on $T(\alpha)$ was transformed in this way and is given in Fig. 15. The numerical values are given in Table III.

The most striking feature of Fig. 15 is the almost triangular appearance of $\bar{F}(\alpha)$ on this semi-log plot. As we shall see, this steady exponential decrease in $\bar{F}(\alpha)$ over 150° in phase angle is in marked contrast to the results we have so far obtained for sputtered samples of rock powders.

Our photometry setup is exactly analogous to that for the astronomical photometry of individual lunar features. Therefore, the Lommel-Seeliger dependence of the intensity distribution $I(i,\epsilon,\alpha)$ is to be removed by multiplication by simply $\left[1 + \cos\epsilon \sec i\right]$. We have accumulated data at three wavelengths and at three angles of emergence ϵ for a large number of rock powder samples. In the case to be analyzed here, greenstone powders of selected particle sizes had been sifted in air for

Table III - Removal of Lommel-Seeliger dependence from the data of Rougier on the brightness of the whole moon.

α	$1 - \sin\frac{\alpha}{2}\tan\frac{\alpha}{2}\ln\cot\frac{\alpha}{4}$	$T(\alpha<0)$	$\bar{F}(\alpha)$	$T(\alpha>0)$	$\bar{F}(\alpha)$
0	1.0000	100	100	100	100
5	0.9927	93.8	94.5	92.0	92.7
10	0.9761	78.7	80.6	75.9	77.8
15	0.9532	69.2	72.6	66.7	70.0
20	0.9254	60.3	65.2	58.6	63.3
25	0.8939	53.0	59.3	51.5	57.6
30	0.8594	46.6	54.2	45.3	52.7
35	0.8226	40.9	49.7	40.2	48.9
40	0.7840	35.6	45.4	35.0	44.6
45	0.7437	31.3	42.1	30.8	41.4
50	0.7031	27.5	39.1	27.3	38.8
55	0.6618	24.0	36.3	23.8	36.0
60	0.6198	21.1	34.0	21.1	34.0
65	0.5780	18.5	32.0	18.4	31.8
70	0.5364	16.1	30.0	15.56	29.0
75	0.4953	14.1	28.5	13.30	26.8
80	0.4549	12.0	26.4	11.07	24.3
85	0.4153	10.0	24.1	9.29	22.4
90	0.3768	8.24	21.9	7.80	20.7
95	0.3395	6.79	19.2	6.66	19.6
100	0.3035	5.60	18.4	5.81	19.1
105	0.2691	4.61	17.1	4.92	18.3

Cont'd. on Following Page

Table III (Cont'd.)

α	$1 - \sin\frac{\alpha}{2} \tan\frac{\alpha}{2} \ln \cot\frac{\alpha}{4}$	$T(\alpha < 0)$	$\bar{F}(\alpha)$	$T(\alpha > 0)$	$\bar{F}(\alpha)$
110	0.2363	3.77	16.0	4.05	17.1
115	0.2052	3.08	15.0	3.31	16.1
120	0.1760	2.49	14.2	2.61	14.8
125	0.1489	1.96	13.2	2.05	13.8
130	0.1237	1.51	12.2	1.58	12.8
135	0.1007			1.21	12.0
140	0.0800			0.93	11.6
145	0.0615			0.69	11.2
150	0.0453			0.46	10.1

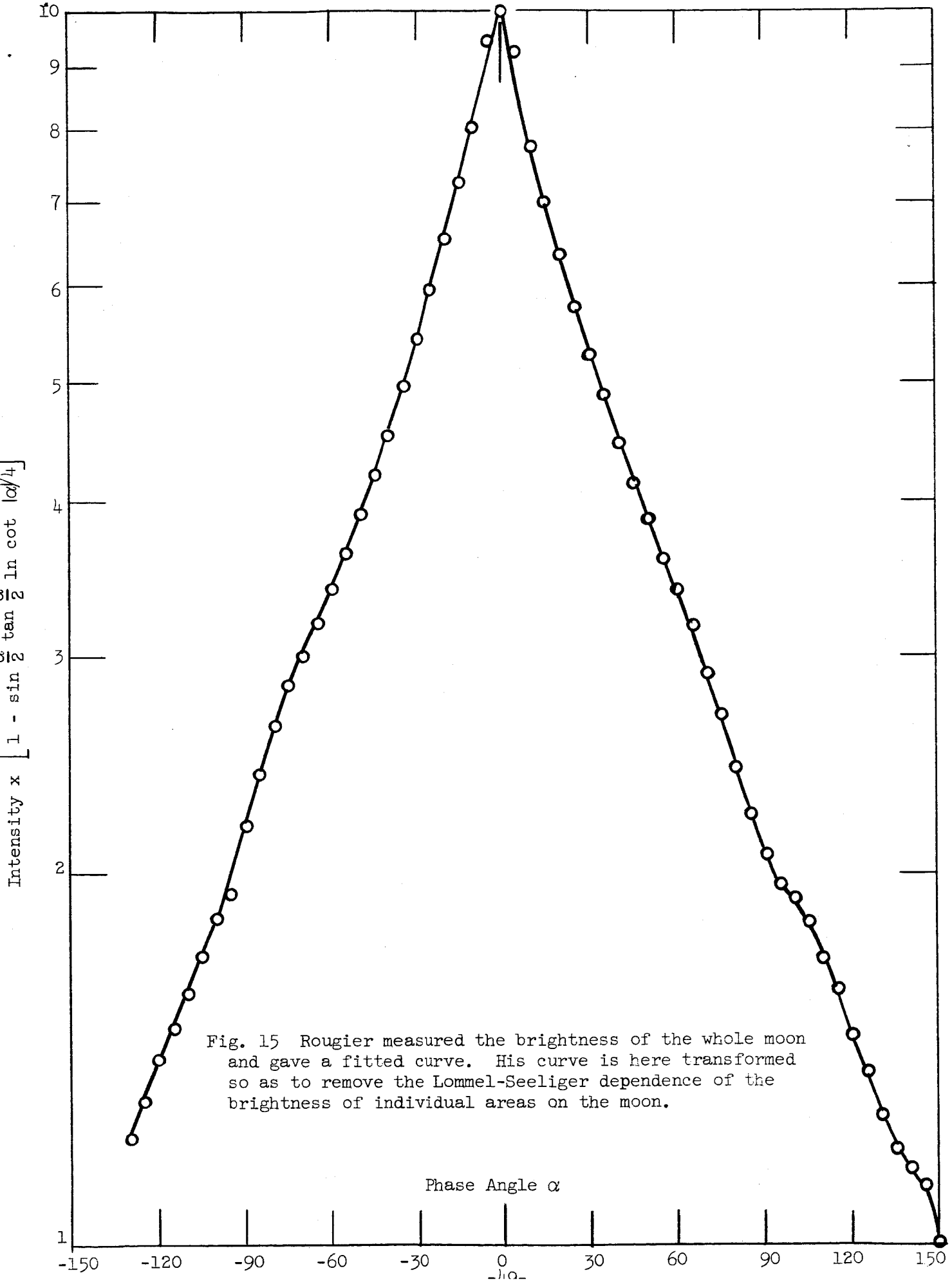

Fig. 15 Rougier measured the brightness of the whole moon and gave a fitted curve. His curve is here transformed so as to remove the Lommel-Seeliger dependence of the brightness of individual areas on the moon.

minimal surface compaction. These powder samples were measured photometrically (and polarimetrically) before and after bombardment by hydrogen ions from an rf discharge plasma. The ion bombardment (at ~500 eV) simulated the sputtering effects to be expected after about 10^4 or 10^5 yr of unprotected exposure of the lunar surface to the solar wind (including the significant sputtering by the He^{++} ions that are estimated to be 15% as abundant as H^+ in the solar wind). The choice of greenstone as the material for study here was convenient because the particles are opaque and the initial albedo exceeds that of an average area on the moon.

What we should expect if $I(i,\epsilon,\alpha) = \left[1 + \cos\epsilon \sec i\right]^{-1} \times F(\alpha)$ is an adequate description of the scattering of light from these tenuous powder surfaces is that the 3 curves for the 3 values of ϵ entering $\left[1 + \cos\epsilon \sec i\right] \times I(i,\epsilon,\alpha)$ should coincide. This should happen for each of the three wavelengths studied and, in fact, the shape of resultant functions should be identical for the three wavelengths as long as multiple scattering and diffraction can be ignored.

In Figs. 16-18, the photometry of sifted 0-20 μ greenstone powder is presented after multiplication by $1 + \cos\epsilon \sec i$. The ordinate is logarithmic, as usual, so a vertical displacement of the curves is not significant.

Figure 16 shows that as ϵ assumes 3 successive values for a given sample, differently shaped curves are obtained for $\left[1 + \cos\epsilon \sec i\right] \times I(i,\epsilon,\alpha)$. This means that the scattering of light from these samples is not adequately described by $I(i,\epsilon,\alpha) = L(i,\epsilon)F(\alpha)$, $L = \left[1 + \cos\epsilon \sec i\right]^{-1}$. Nevertheless, such a factoring is an increasingly good approximation as

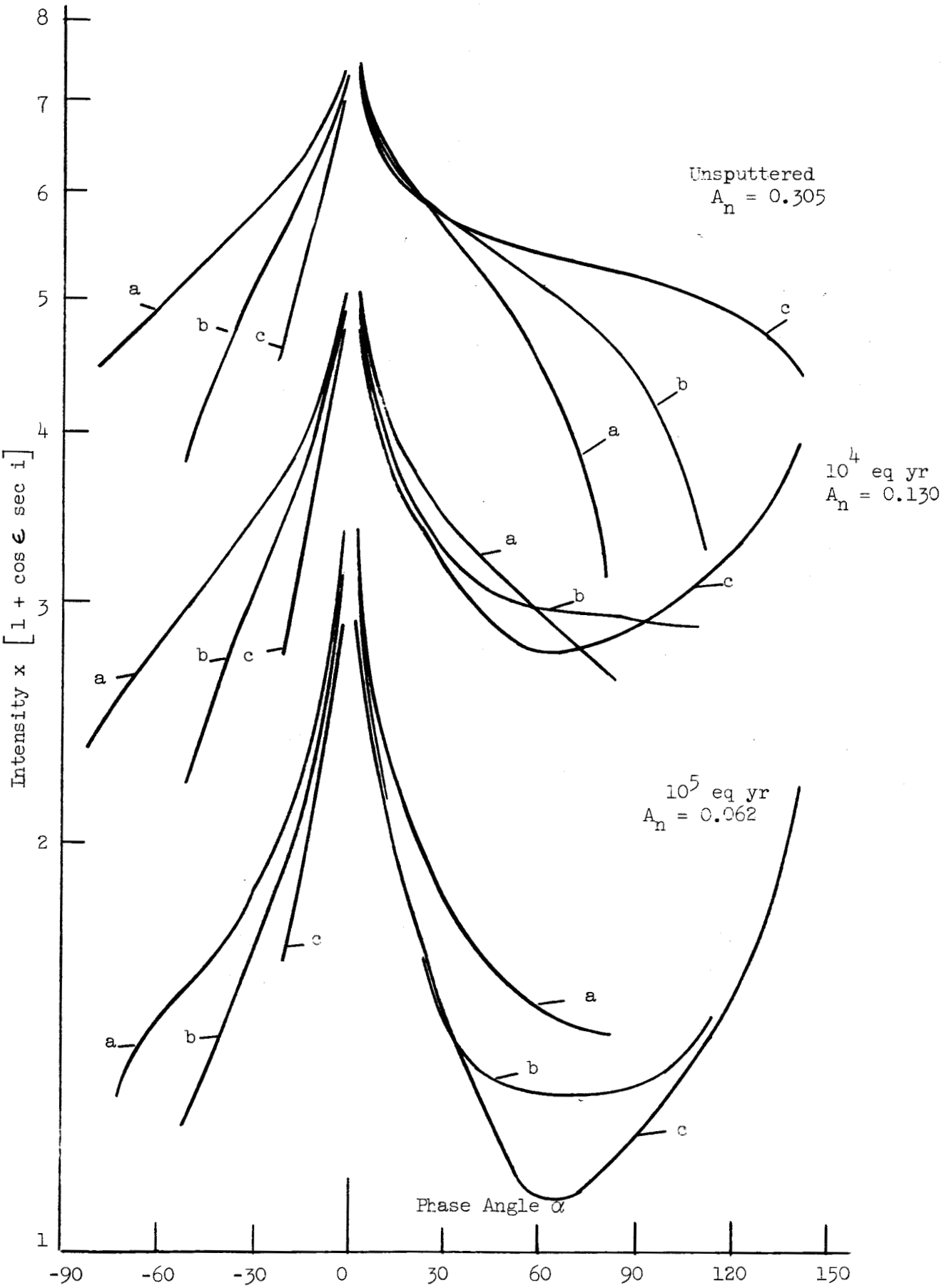

Fig. 16 Photometric function $F(\alpha)$ in red light for sifted 0-20μ greenstone powder. a) $\epsilon = 60°$, b) $\epsilon = 30°$, c) $\epsilon = 0°$. Note how the curves for the three values of ϵ assume increasingly similar shapes as sputtering darkens the surface.

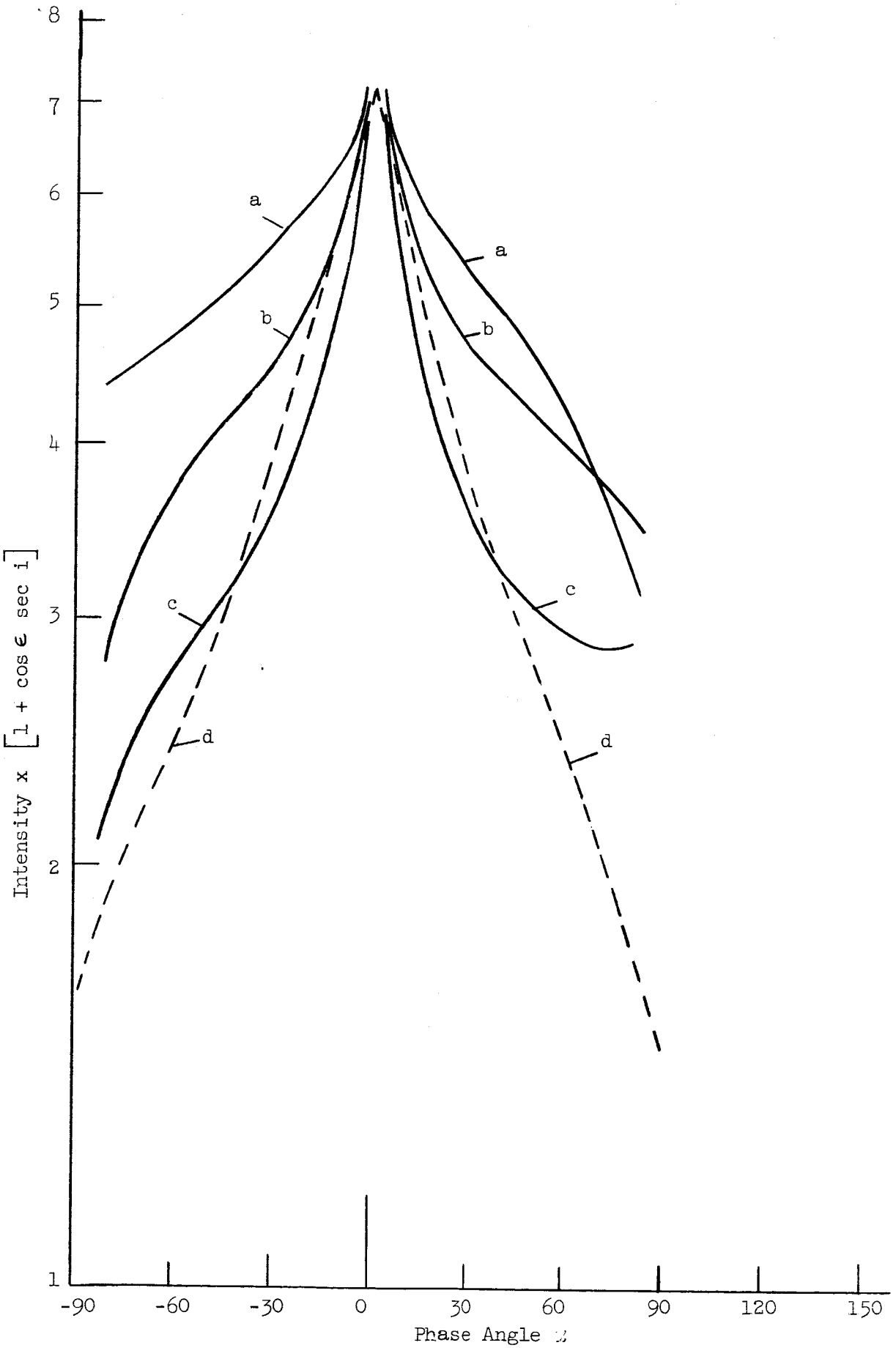

Fig. 17 Change of photometric function $F(\alpha)$ in green light at $\epsilon = 0°$ as sputtering reduces albedo of sifted 0-20 μ greenstone powder. a) A_n = 0.29, unsputtered, b) A_n = 0.11, 10^4 eq yr, c) A_n = 0.049, 10^5 eq yr, d) $\bar{F}(\alpha)$ from lunar data of Rougier.

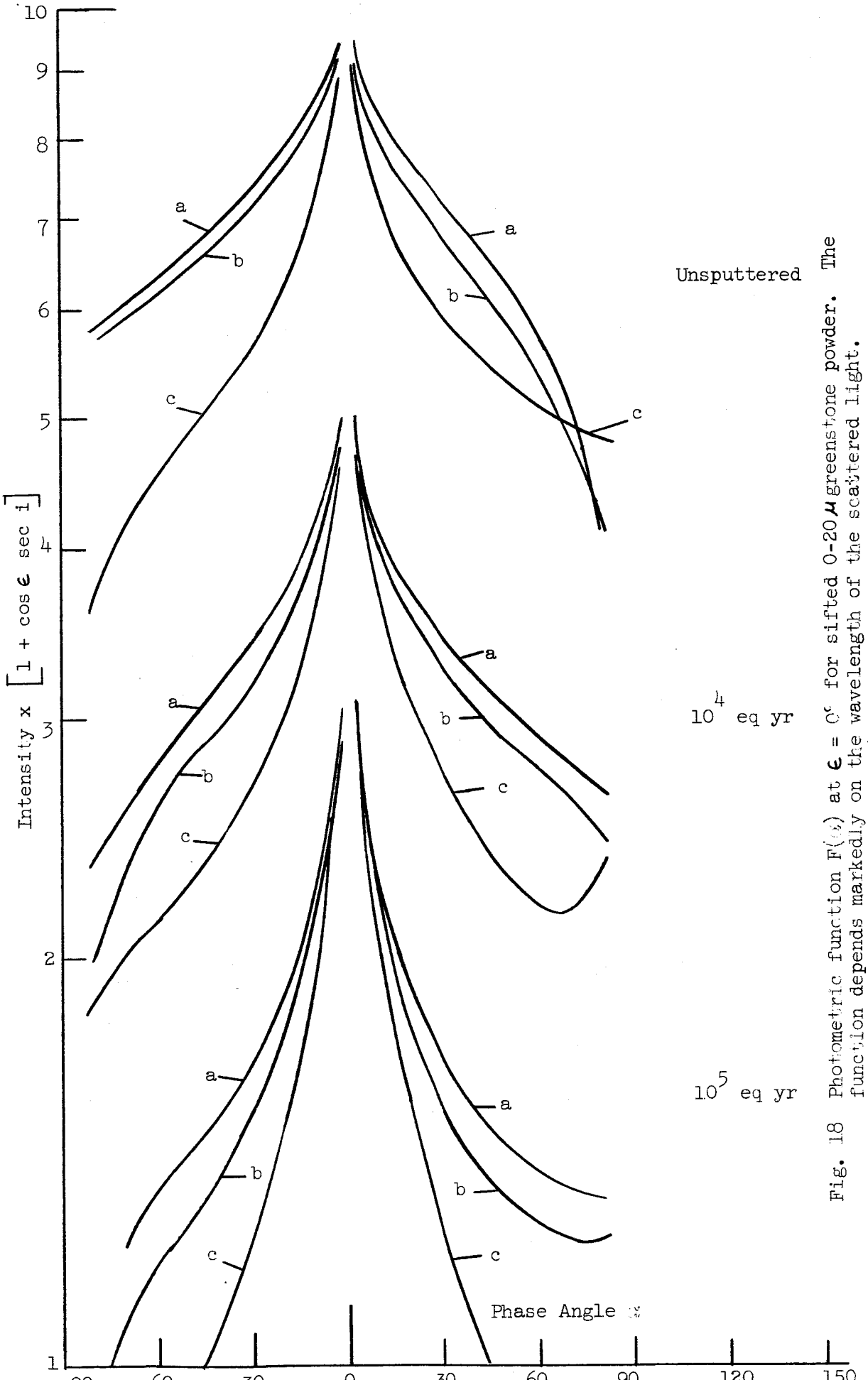

Fig. 18 Photometric function $F(\epsilon)$ at $\epsilon = C^{\epsilon}$ for sifted 0-20 μ greenstone powder. The function depends markedly on the wavelength of the scattered light. a) Red light, b) Green light, c) Ultraviolet light.

sputtering reduces the sample albedo from 0.305 (original) to 0.062 (after the equivalent of about 10^5 yr).

Let us note from Fig. 16 that quite subtle departures from Lommel-Seeliger scattering can be detected by our procedure. For $\epsilon = 30°$ (curves marked "b") the direction of specular reflection is $\alpha = +60°$ while for $\epsilon = 60°$ (curves marked "c") it is $\alpha = +120°$. Note that for the sputtered samples, the $\epsilon = 30°$ curves have a relatively flat region near $\alpha = 60°$ as though scattering is slightly enhanced in the direction of specular scattering. Enhancement of the $\epsilon = 60°$ curve near $\alpha = 120°$ is not distinguishable here but is obvious in scattering from samples containing larger particles. The upward sweep of the $\epsilon = 60°$ curve at $\alpha > 60°$ is not due to specular scattering since the upward trend at $\alpha > 60°$ is also present in the $\epsilon = 30°$ curve.

2. The Presence of Multiple Scattering

In Fig. 17 we analyze just the $\epsilon = 0°$ curves as a function of sample albedo. We find that the unsputtered sample (curve "a") has a broad peak but that the peak becomes more narrow as albedo is reduced. This change in peak shape suggests that multiple scattering in the sample surface is by no means negligible. For if the photometric function depended only upon single scattering and shadowing effects, a decrease in the reflectivity of each particle in the visible surface by a fixed fraction would simply reduce the scattered energy by that fraction. The shape of the photometric function would not be changed. Multiple scattering would broaden the peak but would become relatively less important as the albedo is decreased.

Unfortunately, another effect peculiar to our method of sample darkening can equally well account for the phenomenon evidenced in Fig. 17. Multiple scattering would be the only possible cause of the change in peak shape if and only if the reflectivity of each particle were changed by a fixed fraction. We know, however, that darkening is greatest for the uppermost particles and decreases to no darkening at the greatest depth visible in the sample. Because of shadows, it is improbable that that greatest depth will be illuminated at large phase angles. But as the phase angle decreases toward zero, the greatest depth contributing to the observed light will increase, on the average. Because the more deeply located particles are brighter, the sample effectively has an albedo dependent on phase angle such that the sample looks brighter at small phase angles.

Furthermore, this anomalous change in peak shape would occur at any angle of incidence for a tenuous surface layer because, as is argued in the next section, the effect of shadows at small phase angles depends only upon the phase angle. In Fig. 16 it can be seen that the narrowing of the photometric peak at small phase angles occurs at all three values of ϵ.

In Fig. 17 comparison is made to the lunar data on $F(\alpha)$ by showing Rougier's curve from Fig. 15. The nearly linear lunar curve is in marked contrast to the sample data. Therefore, a "best" fit is hard to justify. In terms of the slope of the curves at $\alpha = 20°$ (where instrumental effects due to finite source and detector angles should be negligible), the darkened samples exhibit better agreement with the lunar data than the unsputtered

sample. Obviously the sample data near glancing incidence is not to be relied on because the curves are not symmetric about $\alpha = 0$. The asymmetry results, of course, from the fact that the sample surface is neither level nor smooth. The disturbing trend for the sample $F(\alpha)$ to curve upward in Fig. 17 is especially obvious in Fig. 16 when the $\epsilon = 30°$ and 60° data is taken into account. This very great discrepancy with the lunar data will be treated below.

3. The Absence of Effects Due to Diffraction and Differing Darkness with Depth

In Fig. 18 the photometric data for $\epsilon = 0°$ is analyzed to determine the effect of varying the wavelength of the scattered light. Whether the sample is sputtered or not, the shape of the photometric peak depends markedly on color of the light. Part of the variation in peak shape for the unsputtered sample can be discounted as due to viewing a slightly different area on the sample. The sample is moved in the course of the usual procedure in order to measure the sample brightness relative to a MgO reference. While care is taken to restore the sample position and orientation, discrepancies in the viewed area evidently occur. Nevertheless, the tendency in Fig. 18 is that which we find in general: the peak in $F(\alpha)$ is narrowest in ultraviolet light and broader with increasing wavelength.

Before further comment on Fig. 18, notice from Fig. 19 that the sample albedo increases steadily from ultraviolet toward the red. Therefore a wavelength change is equivalent to an albedo change unless diffraction effects are important. Diffraction becomes more important

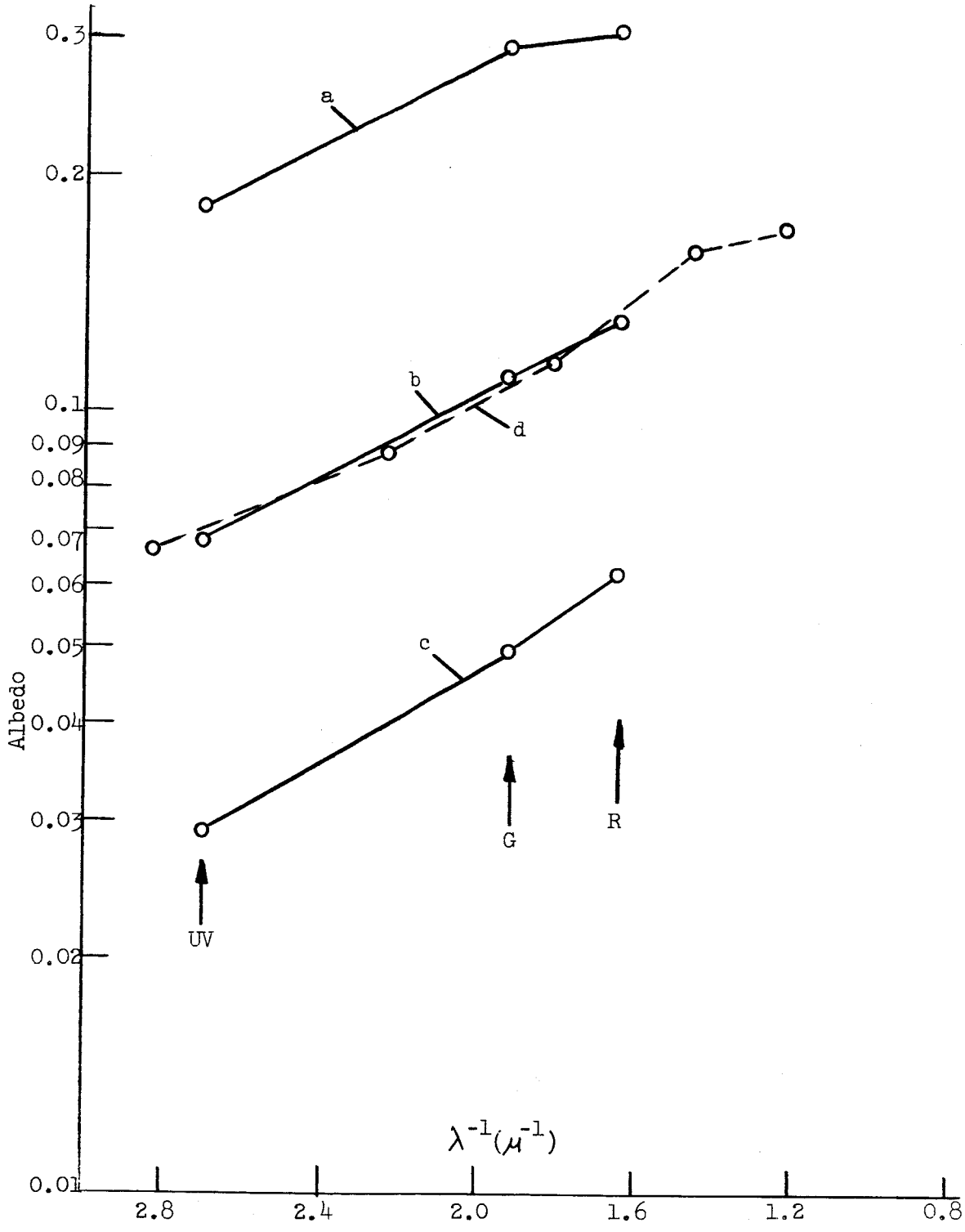

Fig. 19 Albedos of sifted 0-20 μ greenstone powder at 2.5° phase angle. a) Unsputtered, b) 10^4 eq yr, c) 10^5 eq yr, d) Mean albedo of moon at zero phase angle as given by Harris.[20]

as $a \cdot \lambda^{-1}$ decreases, where a is the radius of a particle. Since the distribution of particle sizes in our 0-20 μ sample surely includes particles whose radius is comparable to the wavelength of the scattered light, diffraction might be important.

It is easy to show that diffraction is not noticeably affecting the shape of the peak in the photometric function for our sample of 0-20 μ particles. In Fig. 20, particles of sizes between 20 and 44 μ are studied analogously to Fig. 18. It is obvious that the two figures are very similar. That is, the shape of the peak in the photometric function clearly depends upon the wavelength of the scattered light used to determine it, whether the particle distribution is 0-20 μ or 20-44 μ.

The albedos of the sample of 20-44 μ particles are given in Fig. 21. In general, the behavior of the albedos is very similar to that of the 0-20 μ particles as given in Fig. 19. One can notice that the 20-44 μ sample was initially darker but that after 10^5 eq yr it had not darkened as much as the 0-20 μ sample.

The overlapping of albedos in Fig. 21 suggests that we compare the photometric functions of the 20-44 μ sample at similar albedos, namely, (1) unsputtered sample in ultraviolet light and 10^4 eq yr sample in red light, (2) 10^4 eq yr sample in ultraviolet light and 10^5 eq yr sample in green light. This comparison is made in Fig. 22. In case (1) the agreement is not very good: the peak is broader after sputtering. But in case (2) the agreement is startingly good. The small discrepancies that appear at $|\alpha| > 30°$ are principally due to viewing slightly different areas, as

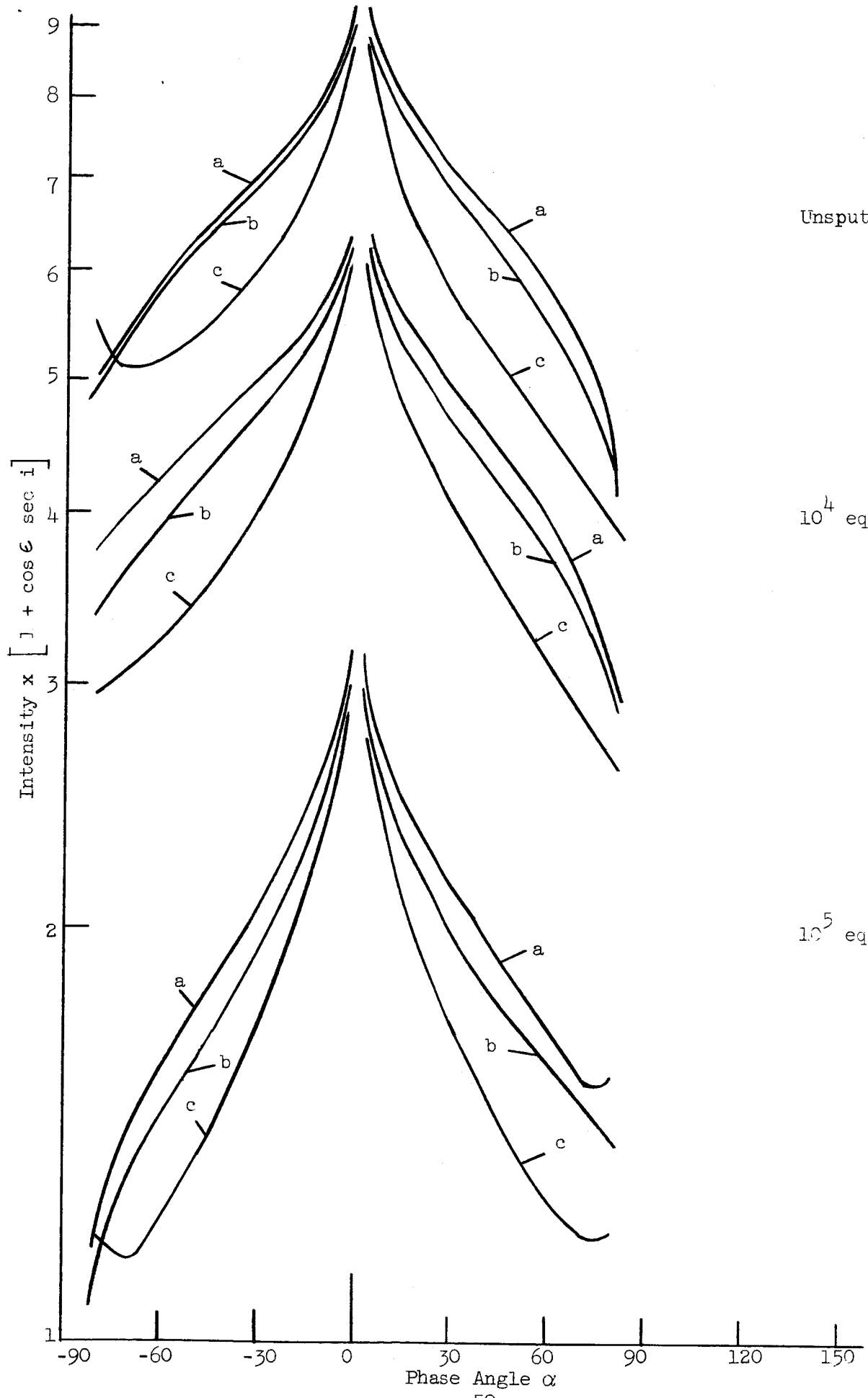

Fig. 20 Photometric function F(α) at ϵ = 0° for sifted 20-44μ greenstone powder. The shape of F(α) depends on wavelength of scattered light very similarly to that for 0-20μ particles. a) Red light, b) Green light, c) Ultraviolet light.

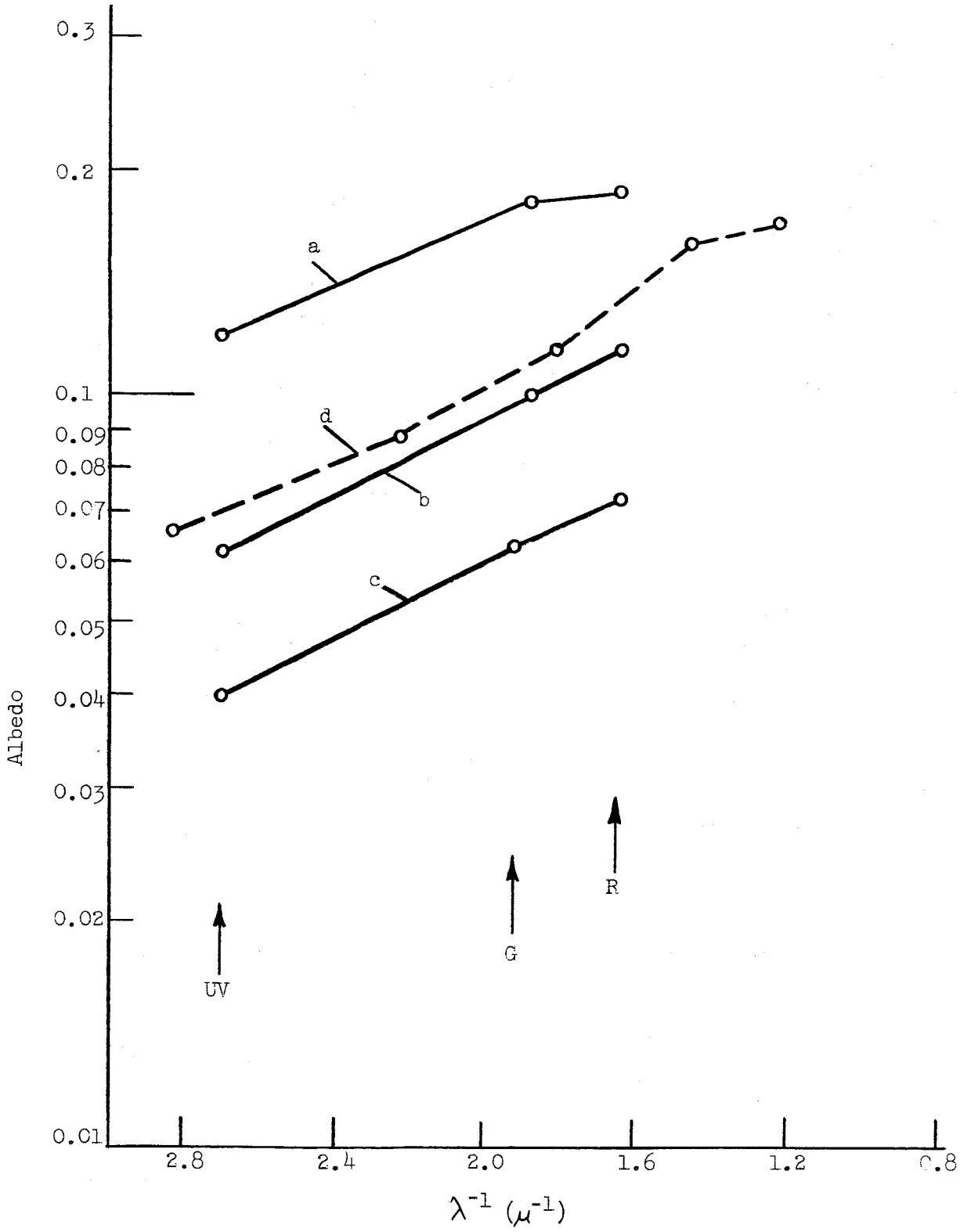

Fig. 21 Albedos of sifted 20-44 μ greenstone powder at 2.5° phase angle. a) Unsputtered, b) 10^4 eq yr, c) 10^5 eq yr, d) Mean albedo of moon at zero phase angle as given by Harris.[20]

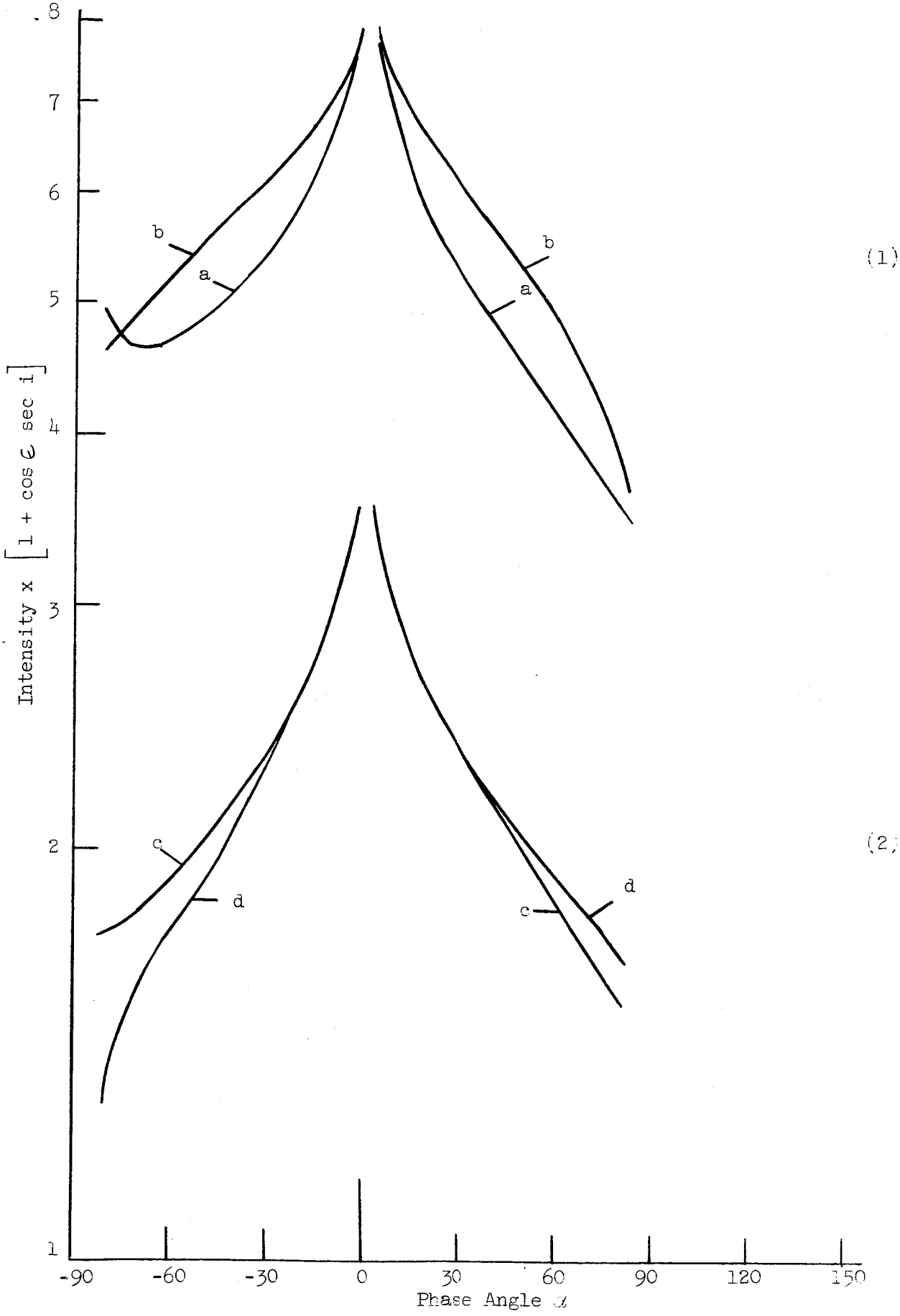

Fig. 22 Photometric functions F(α) at ϵ = 0° for sifted 20-44 μ greenstone powder compared at equal brightnesses at α_1 = +2.5°. a) Unsputtered, UV A_n = 0.120, b) 10^4 eq yr, red A_n = 0.115, c) 10^4 eq yr, UV A_n = 0.062, d) 10^5 eq yr, green A_n = 0.063.

the asymmetries show. Notice that the asymmetries are reversed so that agreement in the shape of the peaks is even better than indicated in Fig. 22.

Let us consider whether differences in darkening with depth could influence the peak in the photometric function as a function of wavelength, namely, whether color differences influence the peak shape. To make the matter obvious, suppose the original sample were bluish but that sputtering gave the uppermost (dark) particles a reddish hue. In red light the upper particles scatter into the detector at all phase angles but the interior, which is viewed at small phase angles, is relatively dark; therefore the peak in red light would be broad. But in blue light the upper particles are especially dark while the interior is relatively bright, so the peak in blue light would be narrow.

In fact, sputtering does make greenstone powder slightly redder, as the steepening slopes in Figs. 19 and 21 reveal. The change in the slopes (colors) in Figs. 19 and 21 are very small relative to the initial slopes, however. Color changes with depth are, at best, a second order effect. It is true that in case (1) in Fig. 22, sputtering seemed to make the peak broader in just the manner outlined above. But since the changes in shape of the photometric peak also occur for the unsputtered sample in Figs. 18 and 20, the change in peak shape of case (1) in Fig. 22 must be discounted as due to some other cause. It could be, for example, the result of an increase in the surface compaction due to jarring the sample. An increase in compaction would be expected to broaden the photometric peak. We conclude that apparent changes in the shape of the photometric peak as a

function of light wavelength are due to differences in particle reflectivities but not significantly due to diffraction or to varying coloration of the particles with depth in the sample.

4. Consequences of Strong Electric Fields During Bombardment of Powders

Additional information could be obtained on systematic consequences of different darkening with depth in our samples by measuring the sample brightness and color at small (preferably zero) phase angle as a function of emergence angle. As the angle of emergence increases, it is to be expected that self-shadowing will confine detected light to that coming from the uppermost particles. If each particle at a given depth were uniformly darkened on its whole surface, then we would expect the surface to look darker at large emergence angles. Secondly, if each particle were uniformly reddened, then we would expect the surface to look more reddish at large emergence angles. The first effect would be equivalent to "limb darkening" while the second would be "limb reddening". Experimentally we find limb brightening instead because of a competing effect.

In the photometric procedure used for these greenstone powder samples, some data were obtained on the brightnesses at, say, $\alpha = 2.5°$ at different values of the emergence angle ϵ. We determined the brightness at $\alpha = 2.5°$ relative to the MgO standard and could have then quickly shifted the detector and light source to $\epsilon = 30°$ or $60°$. Thus the limb darkening for a given color would have been obtained. From the limb darkening at different wavelengths, the colors at each value of ϵ could

have been obtained by intercomparison to the color at $\epsilon = 0°$. In fact, the detector gain was not changed upon changing ϵ nor was the light source intensity modified, but no special precautions were taken to avoid small drifts in making the intensity measurements at $\epsilon = 30°$ and 60°. Therefore, our data permit only semiquantitative statements about limb darkening. The data are not sufficiently reliable to permit analysis of color changes as a function of ϵ.

Both the 0-20 and 20-44 μ samples exhibit about 5% (10%) limb darkening at $\epsilon = 30°$ (60°) in all colors before sputtering. Such limb darkening is to be expected since the samples were not Lommel-Seeliger scatterers (in the sense that I = L x F) on the basis of the test posed in Fig. 16. But the unsputtered samples exhibit appreciably less limb darkening than would have occurred for a diffuse (Lambertian) scatterer for which the brightness is proportional to cos i. After sputtering for 10^4 eq yr, the limb darkening for the 0-20μ sample became less than 1-2% and after 10^5 eq yr, it became a limb brightening by 15-20% at $\epsilon = 60°$. The limb darkening of the 20-44 μ sample was hardly changed by sputtering: an increase of limb darkening to 15% at $\epsilon = 60°$ after 10^5 eq yr may be real.

We believe the limb brightening in the 0-20 μ sample is the consequence of the growth of vertical spires and needles on the surface of the sample and that the expected limb darkening from different darkening with depth is a much smaller effect. We have in various ways detected large forces on particles in a plasma sheath. Lifting forces on the powder particles of our samples are by no means surprising. Just as the

plates of a charged condenser are attracted to each other, so the particles are lifted by electric fields at the plasma boundary. The situation is made slightly more complicated when sputtering is accomplished with alternating fields of radio frequency in that the particles cannot move far in a single cycle. That very fact, however, permits understanding why it is especially needles of conducting material that tend to become aligned along the average field. Suppose that a wire shorter than the condenser plate spacing is fastened at one end to one of two condenser plates, that the wire is otherwise free to move, and that it is subject to no outside forces (gravity, etc.). When the condenser is charged, the free end of the wire will immediately begin to move to align the wire with the electric field. Ignoring inductance effects (a transient magnetic field), the free end of the wire remains at the same potential as the plate to which the wire is fastened. A large electric field occurs at the free end of the wire. A large surface charge occurs on the free end to satisfy the boundary conditions on the wire. Therefore the position of lowest potential energy for the wire is aligned along the electric field. In the "condenser" that the plasma sheath constitutes, the sample surface is negatively charged by the impressed rf field for almost all of a cycle. Only for about $(m_e/m_i)^{\frac{1}{2}} = (1/2 \times 1840)^{\frac{1}{2}} \simeq$ 1/60 of a cycle is the surface charged slightly positive with respect to the hydrogen plasma so as to draw electrons to the surface. Due to this greater mobility of the electrons in the plasma sheath, the average voltage of the surface is essentially half the peak plasma-to-surface voltage.

The effect of substituting a particle of small conductivity for the wire of the previous example is that voltage develops along the particle as the charges flow along it to the tip. Forces would be smaller as a consequence. What we find experimentally is that the tendency to grow aligned spires and needles is far greater for conducting powders (e.g., CuO reduced to Cu by hydrogen sputtering).

The effect of particle size in the case of rf sputtering is that the smallest particles tend to be aligned. This is because the particles intercept a current proportional to an area during the part of the cycle in which electrons are collected. But the particle weight is proportional to a volume. Therefore the ratio of electric to gravitational force is inversely proportional to a particle dimension and larger for the smaller particles. Therefore it is not surprising that it is the 0-20 μ sample that exhibits the anomalous behavior with respect to limb darkening. That sample has a copious supply of particles that can become aligned in the plasma sheath. We have noticed that samples of materials that tend to grow metallic vertical spires exhibit extremely pronounced limb brightening. Apparently the invisible particles being aligned on the 0-20 μ greenstone powder sample are similarly bright when viewed from the side along the direction of illumination.

The polarimetry of these samples has been reported earlier.[21] At small phase angles at both $\epsilon = 0°$ and $\epsilon = 60°$, the polarization exhibited shifts that we at that time attributed to the aligned ion bombardment. The shifts are small for the 20-44 μ sample, but are large for the 0-20 μ sample. It was also the 0-20 μ sample that exhibited the

anomalous limb brightening. We spoke of scattering influenced by "vertical shadows in the scatterer". It now appears that the polarization was affected by aligned particles in the vertical direction. In future studies of darkening with the ion beam apparatus, electric fields at the sample surface will be orders of magnitude smaller than in the plasma sheath.

5. The Problem of $F(\alpha)$ at Phase Angles Greater Than 90°

Our observation of an increasing $F(\alpha)$ at large phase angles is still problematic in view of the steadily decreasing $\bar{F}(\alpha)$ inferred for the moon. In Fig. 23 some data are presented for the 0-20 μ sample that argue against diffraction having any influence on our observations. As in Fig. 22, a comparison is made between the functions $F(\alpha)$ at different wavelengths for which the sample brightnesses are nearly equal at $\alpha = 2.5°$. First of all, the $\epsilon = 0°$ curve in ultraviolet (or red) light agrees very well with the $\epsilon = 60°$ curve at this albedo level. This means that the sample is a very good Lommel-Seeliger scatterer. Second, the $\epsilon = 0°$ curves agree very well in ultraviolet and red light when the albedos in ultraviolet and red light are nearly the same. Therefore diffraction is not important in the $\epsilon = 0°$ curves. Third, the $\epsilon = 60°$ curves are very similar in ultraviolet and red so diffraction is again unimportant in the $\epsilon = 60°$ curves as well. Since $F(\alpha)$ should be given by the product $S(\alpha) \times B(\alpha)$, where $S(\alpha)$ is the scattering function for an average particle and $B(\alpha)$ is a shadowing function that should be quite constant at large phase angles, it follows that $F(\alpha)$ might increase at large phase angles. This is because diffraction

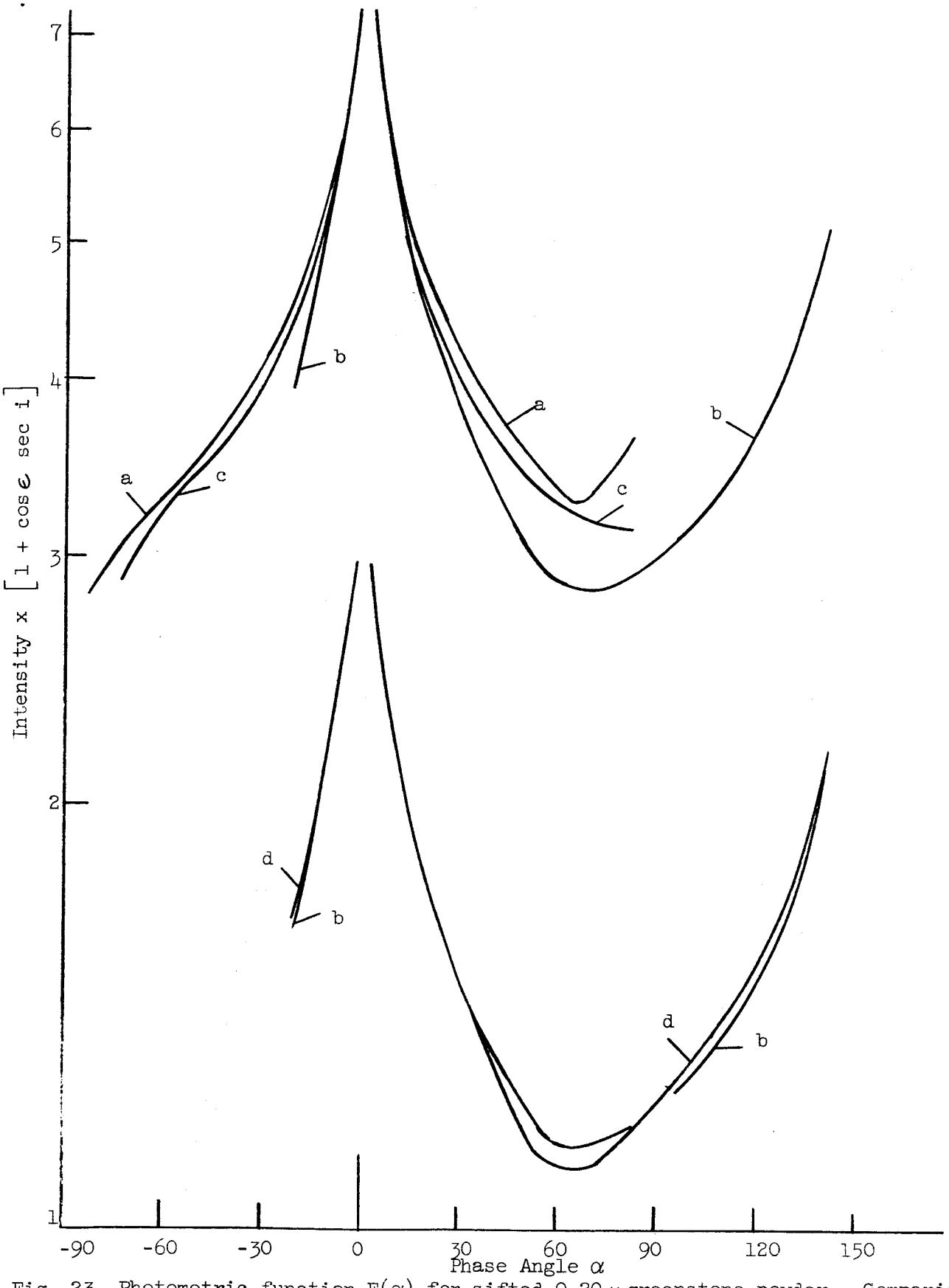

Fig. 23 Photometric function $F(\alpha)$ for sifted 0-20μ greenstone powder. Comparison at 2 wavelengths for which albedos are similar. a) $\epsilon = 0°$ in UV light, 10^4 eq yr, b) $\epsilon = 60°$ in UV light, 10^4 eq. yr, c) $\epsilon = 0°$ in red light, 10^5 eq yr, d) $\epsilon = 60°$ in red light, 10^5 eq yr. The functions are matched at $\alpha = +2.5°$.

scattering entering $S(\alpha)$ is predominantly forward so that $S(\alpha)$ could increase near $\alpha = 180°$. But diffraction would depend strongly on the wavelength of the scattered light, contrary to Fig. 23.

It is easy to see that a decreasing darkening of particles with depth in the sample surface would tend to decrease $F(\alpha)$ at large phase angle rather than increase it. At large angles of incidence and emergence, only the uppermost and darkest particles should contribute to the scattering.

Therefore we conclude that our increasing $F(\alpha)$ at large phase angles probably arises from some undetected systematic error since there does not seem to be any physical reason for the increase. A suitable example might be scattered light from the sample dish which is, after all, much lighter in shade than the low-albedo powder. Additional precautions against stray light will be investigated in the future.

6. Conclusions From Laboratory Photometry

We conclude that low density surfaces of opaque particles are good Lommel-Seeliger scatterers when the particle reflectivities are sufficiently small to make multiple scattering of light unimportant. Removal of the Lommel-Seeliger dependence of the scattering allows detailed study of the remaining function of phase angle, $F(\alpha)$. This function is peaked at small phase angles with a shape governed by surface structure and multiple scattering, but not affected by diffraction or (in our case) varying darkening of the particles with depth in the sample.

The shape of the photometric curve was in fair agreement with the lunar photometric function providing (1) the surface was sifted in air for minimal compaction and (2) the surface had an albedo approximating that of the moon. We find some evidence suggesting the growth of aligned microscopic spires and needles on our samples due to forces arising in the plasma sheath above our samples.

D. Theory and Discussion

The numerous efforts up to 1960 to give a photometric formula for the moon are reviewed by Minnaert.[22] All those efforts were quite unsuccessful, either having no theoretical basis or giving poor agreement with observation. To make theoretical matters worse, in 1964 Gehrels, Coffeen, and Owings published the paper (GCO) whose photometric data we re-analyzed in Section B. They established a detail in the change of lunar brightness with phase that was previously unknown. On a plot of the brightness of the whole moon on a logarithmic scale (brightness in stellar magnitudes, for example), the generally linear course of the data for $|\alpha| \gtrsim 10°$ may not be linearly extrapolated to $\alpha = 0$. Instead, the brightness surges upward at smaller phase angles to what seems to be, from Figs. 3-13, another linear section of higher slope. This feature at small phase angles, as we saw in Fig. 14, is not unconfirmed in earlier data but it was not known to be real.

In 1963, B. Hapke published his important suggestion that the lunar photometric function is factorable: $I(i,\epsilon,\alpha) = L(i,\epsilon)F(\alpha)$. His starting point was the derivation of the Lommel-Seeliger scattering formula. He

did not try to justify why Lommel-Seeliger scattering should be relevant, nor did he effectively test that the appropriate function $L(i,\epsilon)$ was indeed the Lommel-Seeliger function, $\left[1 + \cos\epsilon \sec i\right]^{-1}$. We have in the previous sections demonstrated that Lommel-Seeliger scattering is, in fact, relevant for scattering from surfaces made up of opaque, low-reflectivitiy particles and relevant to the moon. As Hapke also asserted, we found that the surface must not be packed in the way a gravel pile packs itself or departures from Lommel-Seeliger scattering become obvious as enhancements in the scattering in the direction of specular reflection. No such enhancements have been detected for the moon, though the previous methods of analysis may not have been sufficiently precise. The best candidate for showing a specular component in GCO is Copernicus (Fig. 5) because its longitude is less than 30° and its latitude is small. Our analysis indicates no specular component for Copernicus.

We here try to indicate why Lommel-Seeliger scattering should be relevant to light scattering from underdense powders of opaque particles and why multiple scattering in such powders causes departures from Lommel-Seeliger scattering. The Lommel-Seeliger function arises when light is scattered within the bulk of a medium that absorbs light exponentially and isotropically. The energy reaching a detector of area a from the scattering in a volume dV at a depth z below the surface is given by

$$dE = I_o \exp\left[-z \sec i/\tau\right] \times n\sigma\, dV \times bS(\alpha) \times \exp\left[-z \sec\epsilon/\tau\right] \times \frac{a}{r^2} \qquad (5)$$

where I_o is the incident intensity, τ is the absorption length, b is the particle reflectivity, and r is the distance from detector to scattering volume. Replacing dV/r^2 by $\omega\, dr$, where ω is the solid angle subtended at the detector, and introducing the distance R from detector to the point at which the scattered light emerges from the surface, we obtain

$$dE = I_o\, \omega\, abS(\alpha)\ x\ n\sigma\ x\ dr\ \exp\ \left[-\beta(r-R)/\tau\right] \qquad (6)$$

where $\beta = \cos\epsilon\ (\sec i + \sec\epsilon) = 1 + \cos\epsilon\ \sec i = L^{-1}(i,\epsilon)$. Upon integration from R to ∞, the net detected energy is

$$E = I_o\, \omega\ abS(\alpha)\ x\, n\sigma\tau\ x\ L(i,\epsilon)\ . \qquad (7)$$

If, now, the absorption is identified as being due to the scattering taking place, one sets $n\sigma\tau \cong 1$. This final step is crucial because it brings (5) into the form

$$dE \propto \tau^{-1}\ dz\ \exp\ \left[-\tau^{-1}\ z(\sec i + \sec\epsilon)\right]\ . \qquad (5a)$$

Before identification with scattering from powders, let us turn from consideration of exponential absorption by a continuous medium to a model of discrete layers of absorptive "particles".

Imagine a series of horizontal planes separated by a vertical distance D. In each plane let the fraction of the area that is opaque be A_1 and the transparent fraction be A_2. Number the planes from top to bottom. One might desire to vary the opaque area in each plane. Then two indices are needed: A_{1j} and A_{2j}, etc. Apart from shadowing effects of higher layers, the light scattered upward by the j^{th} layer is proportional to A_{1j}. On the other hand, the absorption of light traveling

upward past the j^{th} layer due to scattering from all lower layers is, in general, proportional to A_{1j} also. It is clear that the possibility exists of finding a correspondence between A_{1j} in this model of discrete layers and τ^{-1} in the continuum model.

The coefficient τ^{-1} dz corresponds to the upward scattering per layer in the amount A_{1j} while the absorption per unit length τ^{-1} corresponds to the removal of vertical flux by a factor of A_{1j} per layer.

Note that in the discrete case the probability of penetrating to a depth z is independent of angle of incidence. This is because the probability of penetrating any layer j is A_{2j} on the average. Without absorption between layers, factors of sec i or sec ϵ do not appear. The transition to the continuum case is nevertheless straightforward.

We conclude that Lommel-Seeliger scattering should approximately describe scattering from discrete layers (apart from some multiplying functions arising from particle behavior and shadowing effects) in the following conditions:

1. Tenuous surface - Clearly not even an approximate correspondence of the discrete and continuum cases can be expected if the surface is a solid, opaque plane or even if the surface is rough but made up of particles packed as in a gravel pile. For such surfaces there is no range of angles for which a major portion of the backscattered light is attenuated by passing through a geometrical filter. Instead, such surfaces will exhibit specular scattering to some extent.

2. Small multiple scattering - In the discrete model considered above, if the reflectivity of the opaque areas is high, then an upward flux of light at the j^{th} layer is not simply reduced in transmission by the factor A_{2j}, the open area. Instead, light striking the under side of the area A_{1j} will be scattered downward again. So ultimately some of this multiply scattered light will also pass through A_{2j}. An example is a surface of MgO smoke particles. The surface is formed of discrete particles and is often fairly tenuous. But the reflectivity of each particle is so high that multiple scattering is very prominent. The resulting photometric function is very nearly that of Lambert in which the scattered energy is proportional to $I_o \cos i \cos \epsilon$.

In what follows we will attempt to indicate in terms of the model of discrete layers what effect the shadows introduce as a modification of Lommel-Seeliger scattering. We will not actually propose a photometric function for the moon, as Hapke did, because of the great complexity of the problem. In particular, we know that multiple scattering affects the shape of $F(\alpha)$. However, we will indicate how each of the now known features of the lunar photometric function arise.

The best way to proceed is by the method of induction. In Fig. 24 the upper two layers are indicated. The direct contribution of the first layer to the emerging light is

$$dE_1 = A_{11} \times bS(\alpha) . \qquad (8)$$

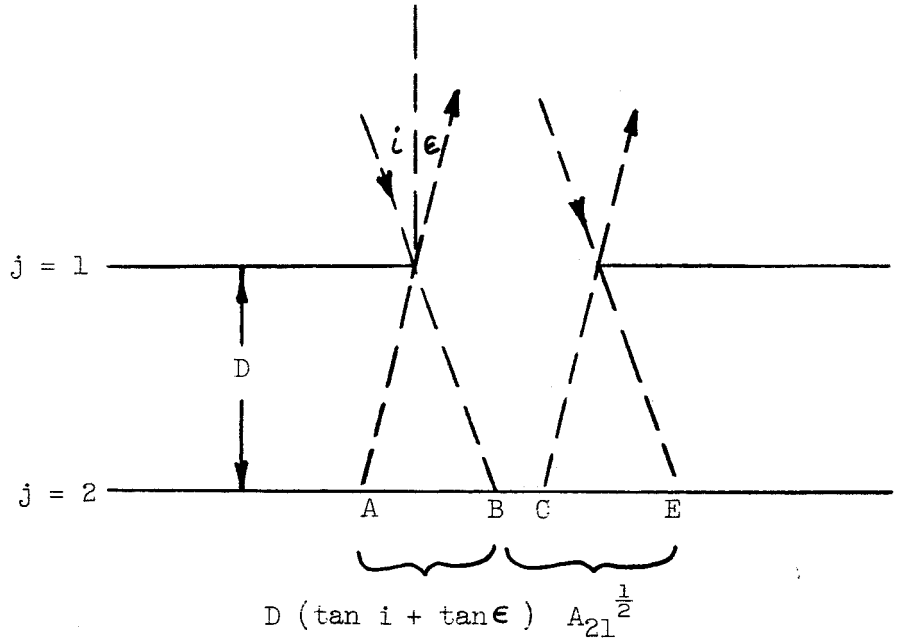

Fig. 24 Diagram of shadows at small phase angles in a model of layered scatterers.

The light penetrating is proportional to $A_{21} = 1-A_{11}$. We assume the positions of the particles in each layer are completely uncorrelated with the other layers. Then the light contributed from the second layer is

$$dE_2 = (1-A_{11}) \times A_{12}\, bS(\alpha) \times X(i,\epsilon) \times (1-A_{11}) \quad . \tag{9}$$

The factor $X(i,\epsilon)$ expresses the fraction of the illuminated area of the second layer that can be seen through the first layer. At $i = \epsilon = 0$ it is clear that $X = 1$. At small i and ϵ, the diagram in Fig. 22 suggests that X decreases as $\left[A_2^{\frac{1}{2}} - D(\tan i + \tan \epsilon)\right] A_2^{-\frac{1}{2}}$. However, such an expression for X will lose its validity as soon as the phase angle is large enough so that light from layer 2 can enter through layer 1 in one hole and later exit through a different hole. Therefore at large phase angles one would expect the shadow pattern on layer 2 to be uncorrelated with the viewing holes in layer 1. The probability that one would then see light through a viewing hole would be simply $(1-A_{11})$. In summary, $X(i,\epsilon)$ should decrease linearly as $(1-\gamma\alpha)$ near $\alpha = 0$, $\gamma \sim DA_2^{-\frac{1}{2}}$, but then it becomes asymptotic to a finite value at large phase angles. The finite value is related to the open area per layer. Clearly the factor $X(i,\epsilon)$ is crucial to the understanding of the backscatter properties of a powder surface.

In writing the light contributed from the j + 1 layer, one will have a product of fractions for the attenuation on entry of the form $\prod_1^j (1-A_{1k})$ which is recognizable as equivalent to an exponential decay

$\exp\left[-(IN)_j\right]$. There is a similar $\exp\left[-(OUT)_j\right]$.

$$dE_{j+1} = \exp\left[-(IN)_j\right] A_{1,j+1}\, bS(\alpha) \times X(i,\epsilon) \times \exp\left[-(OUT)_j\right] \qquad (10)$$

Now if attenuation per layer is not too great (gravel pile packing) the identification of A_{1j} with $\tau^{-1}dz$ and $X(i,\epsilon)$ with $B(\alpha)$ brings us immediately to a modification of Eq. (5a):

$$dE \propto \exp\left[-\tau^{-1} z \sec i\right] \tau^{-1} dz \times bS(\alpha)B(\alpha) \exp\left[-\tau^{-1} z \sec \epsilon\right] . \qquad (11)$$

The most important place multiple scattering is apt to enter as a correction, if the particle reflectivities are quite low, is in glancing reflections from the particles. Such multiple scattering is apt to affect the shape of $B(\alpha)$ at small phase angles by softening shadows and broadening $B(\alpha)$. A small dependence of lunar color upon phase described in GCO is analogous to our finding that the shape of $F(\alpha)$ for laboratory samples depended upon wavelength through a change in particle reflectivity with wavelength. The fact that the moon becomes more reddish as $|\alpha|$ increases reveals that $F(\alpha)$ in blue moonlight has a narrower peak than in red. This is what we find for greenstone and other rock powders. In the previous section we concluded this effect was simply a consequence of multiple scattering. In particular, it is multiple scattering at glancing reflection. Note that multiple scattering at glancing reflection from dark powder grains does not ruin the overall Lommel-Seeliger scattering but shows up instead in $F(\alpha)$.

In Hapke's attempt to formulate this problem, there are the following objections. He tried to account for the discrete nature of the scattering medium by introducing holes into the medium, but assumed absorption upon entry into the holes. Thereupon if scattering led to exit through the entry hole, he assumed zero absorption on exit. Of course, this obvious asymmetry of entry and exit led to an expression violating the reciprocity theorem of Minnaert.[23] Instead of attempting a more symmetric formulation, he simply made an approximate substitution that should be valid only at $\alpha = 0$, if at all. Upon integration, he made some error that led to a function $B(\alpha)$ that happened to be simple and well behaved. He then assumed this $B(\alpha)$ was valid, not only near $\alpha = 0$, but to $\alpha = \pm 180°$. His use of holes corresponds to the representation of $X(i,\epsilon)$ by the linear approximation $X(i,\epsilon) \cong 1 - \gamma\alpha$ that was given above. He completely missed the concept of entry and exit through non-adjacent openings though it contributes dominantly to the lunar $B(\alpha)$ for $|\alpha| > 10°$.

In conclusion, we have offered a justification for the relevance of Lommel-Seeliger scattering to scattering of light from underdense powders of dark, opaque particles. We have suggested the physical basis upon which shadowing effects in a discrete scatterer modify the continuum absorption of Lommel-Seeliger scattering. We have identified the abrupt rise in lunar brightness near phase angle $\alpha = 0$ that was established in GCO[16] as being due to light scattering back through the same opening by which it entered. At larger phase angles the light scattered from the moon generally exits by a path such that an obstruction lies between

the entry and exit path. This requires that voids in the moon's surface layer are interconnected as in a powder.

The fact that Lommel-Seeliger scattering accurately describes the way in which the lunar scattering of light depends upon the angles of incidence and of emergence and that no characteristic departures from L-S scattering near the specular direction can be detected in precision lunar photometry powerfully argues for a layer of underdense powder on the moon. The layer must be thick enough to completely dominate the formation of shadows at the surface.

VI. LIST OF REFERENCES

1. Hapke, B. and H. Van Horn. Photometric studies of complex surfaces with applications to the moon. J. Geophys. Res. 68: 4545-70 (1963).

2. Ruskol, Ye. L. The physical properties of the lunar surface. Cosmic Res. 3, 3: 76-103 (1965). (U. S. Air Force. Systems Command. Foreign Technology Division. Translation FTD-TT-65-828).

3. Jaffe, L. D. Depth of the lunar dust. J. Geophys. Res. 70: 6129-38 (1965).

4. ----. Lunar dust depth in Mare Cognitum. J. Geophys. Res. 71: 1095-1103 (1966).

5. Hagfors, T. et al. Tenuous surface layer on the moon: evidence derived from radar observations. Science 150: 1153-56 (1965).

6. Davis, J. R. and D. C. Rohlfs. Lunar radio-reflection properties at decameter wavelengths. J. Geophys. Res. 69: 3257-62 (1964).

7. Massachusetts Institute of Technology. Lincoln Laboratory. Technical Report No. 272. Radio-echo observations of the moon at 68-cm wavelength, by J. W. Evans (June 22, 1962).

8. Smoluchowski, R. Radiation sintering of lunar dust. Science 150: 1025-26 (1965).

9. Litton Systems, Inc. Applied Science Division. Report No. 2722. Investigation of sputtering effects on the moon's surface. by G. K. Wehner, D. L. Rosenberg, and C. E. KenKnight. Contract NASw-751. Seventh quarterly status report (February 16, 1965).

10. Wehner, G. K. Sputtering by ion bombardment. In Advances in electronics and electron physics, Vol. 7. N.Y., Academic Press, 1955. pp. 239-98.

11. ---- and D. L. Rosenberg. Angular distribution of sputtered material. J. Appl. Phys. 31: 177-79 (1960).

12. Grønlund, F. and W. J. Moore. Sputtering of silver by light ions with energies from 2 to 12 kev. J. Chem. Phys. 32: 1540-45 (1960).

13. Wehner, G. K., C. E. KenKnight, and D. L. Rosenberg. Sputtering rates under solar-wind bombardment. Planetary Space Sci. 11: 885-95 (1963).

14. Guentherschulze, A. Z. Physiz 36: 563 (1926).

15. Blauth, E. W. and E. H. Meyer. Zur Gasaufzehrung in einer HF-Gasentladung. Z. Angew. Phys. 19: 549-52 (1965).

16. Gehrels, T., T. Coffeen, and D. Owings. Wavelength dependence of polarization. III. The lunar surface. Astron. J. 69: 826-52 (1964).

17. Hapke, B. W. A theoretical photometric function for the lunar surface. J. Geophys. Res. 68: 4571-86 (1963).

18. Rougier, G. Total photoelectric photometry of the moon. Ann. Observat. Strasbourg 2, 3: 205-39 (1933).

19. Van Diggelen, J. Photometric properties of lunar crater floors. Rech. Astron. Observat. Utrecht 14, No. 2 (1959). (NASA Technical Translation F-209).

20. Harris, D. L. Photometry and colorimetry of planets and satellites. In Kuiper, G. and B. M. Middlehurst, eds. The solar system: Vol. 3. Planets and satellites. Chicago, University of Chicago Press, 1961. pp. 272-342.

21. Litton Systems, Inc. Applied Science Division. Report No. 2792. Investigation of sputtering effects on the moon's surface, by G. K. Wehner, D. L. Rosenberg, and C. E. KenKnight. Contract NASw-751. Eighth quarterly status report (May 14, 1965).

22. Minnaert, M. Photometry of the moon. In Kuiper, G. P. and B. M. Middlehurst, eds. The solar system: Vol. 3. Planets and satellites. Chicago, University of Chicago Press, 1961. pp. 213-48.

23. ----. The reciprocity principle in lunar photometry. Astrophys. J. 93: 403-10 (1941).